Dynamics in $\mathcal{PT}$-Symmetric Honeycomb Lattices with Nonlinearity

By Christopher W. Curtis and Yi Zhu

We examine the impact of small parity-time ($\mathcal{PT}$) symmetric perturbations on nonlinear optical honeycomb lattices in the tight-binding limit. We show for strained lattices that complex dispersion relationships do not form under perturbation, and we find a variety of nonlinear wave equations which describe the effective dynamics in this regime. The existence of semilocalized gap solitons in this case is also shown, though we numerically demonstrate these solitons are likely unstable. We show for unstrained lattices under the effect of a restricted class of $\mathcal{PT}$ perturbations, which prevent complex dispersion relationships from appearing, that nontrivial phase dynamics emerge as a result of the $\mathcal{PT}$ perturbation. This phase can be understood as momentum imparted to optical beams by the lattice, thus showing $\mathcal{PT}$ perturbations offer potentially novel means for the control of light in honeycomb lattices.

1. Introduction

Over the last several years, researchers in optics have pursued two novel, and increasingly important, lines of research. The first concerns the propagation of light in honeycomb lattices of dielectric material, or "optical graphene." By a honeycomb lattice, we mean two distinguished triangular lattices overlayed on one another. Optical graphene systems are often characterized by the presence of "Dirac-points," or conical intersections, in the dispersion bands associated with the honeycomb lattice, though perturbations can influence

Address for correspondence: Christopher W. Curtis, Department of Mathematics and Statistics, SDSU, 5500 Campanile Dr., GMCS 415, San Diego 92182, USA; e-mail: ccurtis@mail.sdsu.edu

DOI: 10.1111/sapm.12081

STUDIES IN APPLIED MATHEMATICS 135:139–170

the presence of Dirac points. Due to the infinite curvature at these conical intersections, new optical phenomena such as conical diffraction [1], strain induced pseudo-magnetic responses [2], and novel edge states 3–6 have been observed. Beyond visible light phenomena, graphene systems in the microwave regime have also been studied cf. [7–10]. In response to this ever growing body of physical literature, mathematical and theoretical studies of these effects have appeared in Refs. [11–17] and [18, 19].

The second line of research involves optical systems which are, due to carefully introduced gain and loss media, symmetric with respect to parity and time conjugation transformations. These systems are known as parity-time ($\mathcal{PT}$) symmetric systems as introduced in the now seminal paper [20], and as expanded upon both theoretically and experimentally in cf. [21–25]. Phenomena such as novel beam diffraction patterns [24], loss-induced transparency [26], and unidirectional invisibility [27] have been observed. All of this phenomena depends on the fundamental question of whether dispersion relationships remain real in the presence of gain and loss media, or if a "phase transition" [28] has caused dispersion relationships to become complex. For $\mathcal{PT}$-symmetric systems, a phase transition necessarily means an instability has emerged, thus allowing for small perturbations to become large. Establishing whether phase-transitions do or do not occur has been studied in several different contexts, see Refs. [21, 29–33] for example. Note, the phrase "spontaneous symmetry breaking" [34] is sometimes used in place of phase transition, though in this paper we use the latter convention.

There is relatively little work on how $\mathcal{PT}$-symmetric perturbations influence dynamics in optical-graphene systems, or what we call $\mathcal{PT}$-symmetric honeycomb lattices. As Dirac points are isolated degeneracies in the dispersion band associated with the honeycomb lattice, we expect $\mathcal{PT}$-perturbations to separate the Dirac points. The key issue then is whether phase-transitions occur during this separation. To study this, cf. [34–36] introduce $\mathcal{PT}$ perturbations into linear "tight-binding models" of optical graphene. By a tight-binding model, we mean that the potential describing the honeycomb lattice is taken to be deep, which allows continuous in space Schrödinger equations to be well-approximated by infinite-dimensional discrete systems. These models have shown that by introducing enough strain into the lattice, which separates the Dirac points but keeps the dispersion relationship real, phase transitions do not occur for sufficiently weak $\mathcal{PT}$ perturbations [34, 35].

In Ref. [37], the impact of $\mathcal{PT}$ perturbations on linear Schrödinger equations with honeycomb lattice potentials was studied. There it was shown in unstrained lattices that two classes of $\mathcal{PT}$ perturbations exist. For the first class, called "real-mass" potentials, due to extra symmetry, small to even moderately large $\mathcal{PT}$ perturbations separate Dirac points but do not induce phase transitions. In contrast, for the second class, termed "imaginary-mass" potentials, the absence of extra symmetry means that the Dirac points

separate under perturbation into the complex plane, thereby inducing a phase transition.

However, at present, the role of nonlinearity in $\mathcal{PT}$ symmetric honeycomb lattices has not been studied. Therefore in this paper, we study the propagation of nonlinear two-dimensional optical beams in optical graphene under the influence of both real and imaginary-mass perturbations. This is done by finding solutions to asymptotic reductions of a nonlinear Schrödinger equation (NLSE) with added potentials representing the honeycomb lattice and the $\mathcal{PT}$-symmetric perturbation. Modeling nonlinear envelopes over the relatively rapidly varying honeycomb lattice makes even numerical simulations of the NLSE challenging, and deriving analytical results is more difficult still. Thus, we use various asymptotic approximation schemes which produce simpler nonlinear wave equations representing the most important balances between various physical effects. This allows for faster and more standard numerical simulations of phenomena and the derivation of physically meaningful and computable analytical expressions.

For imaginary-mass potentials, this simplification is done via a tight-binding approximation. Using this technique, we derive an infinite dimensional discrete system that balances the effects of dispersion from the Dirac points, gain and loss from the $\mathcal{PT}$ perturbation, and nonlinearity. In the linear regime, we also present a detailed derivation of the results in Refs. [34, 35]. We then look at the case of balancing small, strain induced, gaps between Dirac points against small $\mathcal{PT}$ perturbations in such a way that phase transitions are prevented. In this balance, following Ref. [38], by taking a continuum limit in the discrete system, we derive scalar constant-coefficient nonlinear dispersive wave equations which describe the dominant wave dynamics.

A key feature of nonlinearity is that it allows for the existence of localized, nonlinear modes that persist despite dispersion. In optics, these modes are often referred to as optical solitons [39]. Using the reduced models of the NLSE that we derive allows us to find one-dimensional solitons in the strain-induced gap. We describe these modes as semilocalized gap solitons. We numerically show these solitons are unstable with respect to transverse perturbations. We note that while gap solitons have been shown to exist in honeycomb lattices, cf. [1], these modes were found between higher energy bands. Therefore, to the best of our knowledge, we are presenting the first study of nonlinear modes found in gaps between the lower energy Dirac points, though the idea was discussed in Ref. [38]. The results in this paper hint at the existence of larger families of nonlinear gap modes, and these modes could increase the potential applications of optical graphene. This is a subject of ongoing research for the authors.

For real-mass perturbations, a tight-binding approximation does not readily allow one to capture the higher order effects that influence dynamics. This stems from the fact that while real-mass perturbations separate Dirac points, this separation is much weaker than for imaginary-mass potentials. Instead

of a tight-binding approximation then, we use a slow envelope ansatz as in Ref. [16], where by we derive a constant-coefficient nonlinear Dirac equation describing the effective dynamics of optical beams. In this derivation, we show that real-mass potentials introduce nontrivial spatially varying phases which add momentum to the flow of the beam. This momentum is in addition to the angular momentum resulting from the pseudospin structure [40–42] induced by the honeycomb lattice, a subject of much recent interest. Hypothetically, carefully designed real-mass $\mathcal{PT}$-symmetric honeycomb lattices could be engineered so as to confer a greater degree of control over the flow of light by manipulating these two sources of momentum for optical beams.

In summary, for the two classes of $\mathcal{PT}$ perturbations we show:

- **Imaginary-mass**: By balancing $\mathcal{PT}$ and lattice strain effects, families of nonlinear wave equations are derived as leading order approximations to the NLSE. We demonstrate the existence and study the stability of semilocalized nonlinear modes that emerge as a result of the band gap opened between Dirac points by the lattice strain.
- **Real-mass**: We derive a constant-coefficient nonlinear Dirac equation that describes beam dynamics. Due to the $\mathcal{PT}$ perturbations, a nontrivial phase emerges which imparts a linear momentum onto the optical beam.

We point out that in both the real and imaginary mass cases though we only examine dynamics localized in wavenumber around the Dirac point. Our asymptotics shows that this localization is maintained for small amplitude and sufficiently wide initial conditions. On the other hand, if initial envelopes are not small and broad, energy delocalizes away from the Dirac points due to strong nonlinearity and interesting dynamics such as triangular diffraction appear [43,44]. Addressing this issue is beyond the current scope of this paper.

As to the layout of the paper, we present the background on honeycomb lattices, tight-binding approximations, and $\mathcal{PT}$ symmetry in the remainder of Section 1. In Sections 2 and 3, we present the results concerning imaginary and real-mass potentials, respectively. A Conclusion summarizing our findings, and an Appendix collecting technical information are at the end of the paper.

1.1. Honeycomb lattices, dirac points, and strained lattices

Throughout this paper, we study the NLSE

$$iu_z = -\Delta u + \frac{1}{h^2} V(\mathbf{r})u + i\vartheta W(\mathbf{r})u + \sigma|u|^2 u, \tag{1}$$

where $V(\mathbf{r})$ and $W(\mathbf{r})$ are real, smooth, and periodic functions with respect to the vectors $\mathbf{v}_1$ and $\mathbf{v}_2$. The parameters h and ν are taken to be real and small, while $\sigma = \pm 1$. Note, Equation (1), due to the presence of the potentials $V(\mathbf{r})$ and $W(\mathbf{r})$, is also called a Gross–Pitaevskii (GP) equation. The potential $V(\mathbf{r})$

represents the honeycomb lattice while $W(\mathbf{r})$ represents the $\mathcal{PT}$-perturbation. Using the period vectors $\mathbf{v}_1$ and $\mathbf{v}_2$, we generate a lattice $\mathbb{P}$ where

$$\mathbb{P} = \{m_1\mathbf{v}_1 + m_2\mathbf{v}_2 : m_j \in \mathbb{Z}\}.$$

As a point of reference, we place $\mathbf{v}_1$ and $\mathbf{v}_2$ at the origin and define the primitive cell Ω to be

$$\Omega = \{\kappa_1\mathbf{v}_1 + \kappa_2\mathbf{v}_2 : \kappa_j \in [0, 1]\}.$$

Likewise, we define the dual lattice $\mathbb{P}'$ as the lattice formed by the vectors $\mathbf{k}_j$, defined via the relation $\mathbf{k}_j \cdot \mathbf{v}_l = 2\pi\delta_{jl}$, cf. [45]. We also define the dual primitive cell, Ω', with $\mathbf{k}_1$ and $\mathbf{k}_2$ located at the origin as

$$\Omega' = \left\{\kappa_1\mathbf{k}_1 + \kappa_2\mathbf{k}_2 : \kappa_j \in [0, 1]\right\}.$$

See Figure 1 for reference. By convention, we choose

$$\mathbf{v}_1 = \ell\begin{pmatrix}\frac{\sqrt{3}}{2}\\ \frac{1}{2}\end{pmatrix}, \quad \mathbf{v}_2 = \ell\begin{pmatrix}\frac{\sqrt{3}}{2}\\ -\frac{1}{2}\end{pmatrix}, \quad \ell > 0,$$

which implies then that

$$\mathbf{k}_1 = \frac{4\pi}{\ell\sqrt{3}}\begin{pmatrix}\frac{1}{2}\\ \frac{\sqrt{3}}{2}\end{pmatrix}, \quad \mathbf{k}_2 = \frac{4\pi}{\ell\sqrt{3}}\begin{pmatrix}\frac{1}{2}\\ -\frac{\sqrt{3}}{2}\end{pmatrix}, \quad \ell > 0.$$

We then say that a $\mathbb{P}$-periodic function $V(\mathbf{r})$ is a honeycomb potential if there are two points, say $\mathbf{r}_1 = (x_1, 0)$ and $\mathbf{r}_2 = (x_2, 0)$, $x_2 > x_1$, in Ω such that

- $V(\mathbf{r}_1) = V(\mathbf{r}_2) = 0$, $V(\mathbf{r}) > 0$, $\mathbf{r} \neq \mathbf{r}_j$,
- $V(\mathbf{r})$ is even.

We define the separation vector $\mathbf{d} = \mathbf{r}_2 - \mathbf{r}_1$ between the "wells" $\mathbf{r}_j$ with the requirement that $\mathbf{d} \notin \mathbb{P}$. We say the lattice is "unstrained" if

$$|\mathbf{d}| = |\mathbf{v}_1 - \mathbf{d}|,$$

and "strained" if

$$|\mathbf{d}| < |\mathbf{v}_1 - \mathbf{d}|.$$

So by strain, we mean that we allow the distance between the wells $\mathbf{r}_j$ to decrease while keeping all other parameters of the honeycomb lattice fixed.

Per our choice of lattice vectors $\mathbf{v}_j$ then, the Brillouin zone BZ in the dual lattice, without strain, is an equilateral hexagon, see Figure 1(b). This implies that there are two types of corners of the BZ, say $\mathbf{K}$ and $\mathbf{K}'$, where

$$\mathbf{K} = \frac{1}{3}(\mathbf{k}_1 - \mathbf{k}_2), \mathbf{K}' = -\mathbf{K}.$$

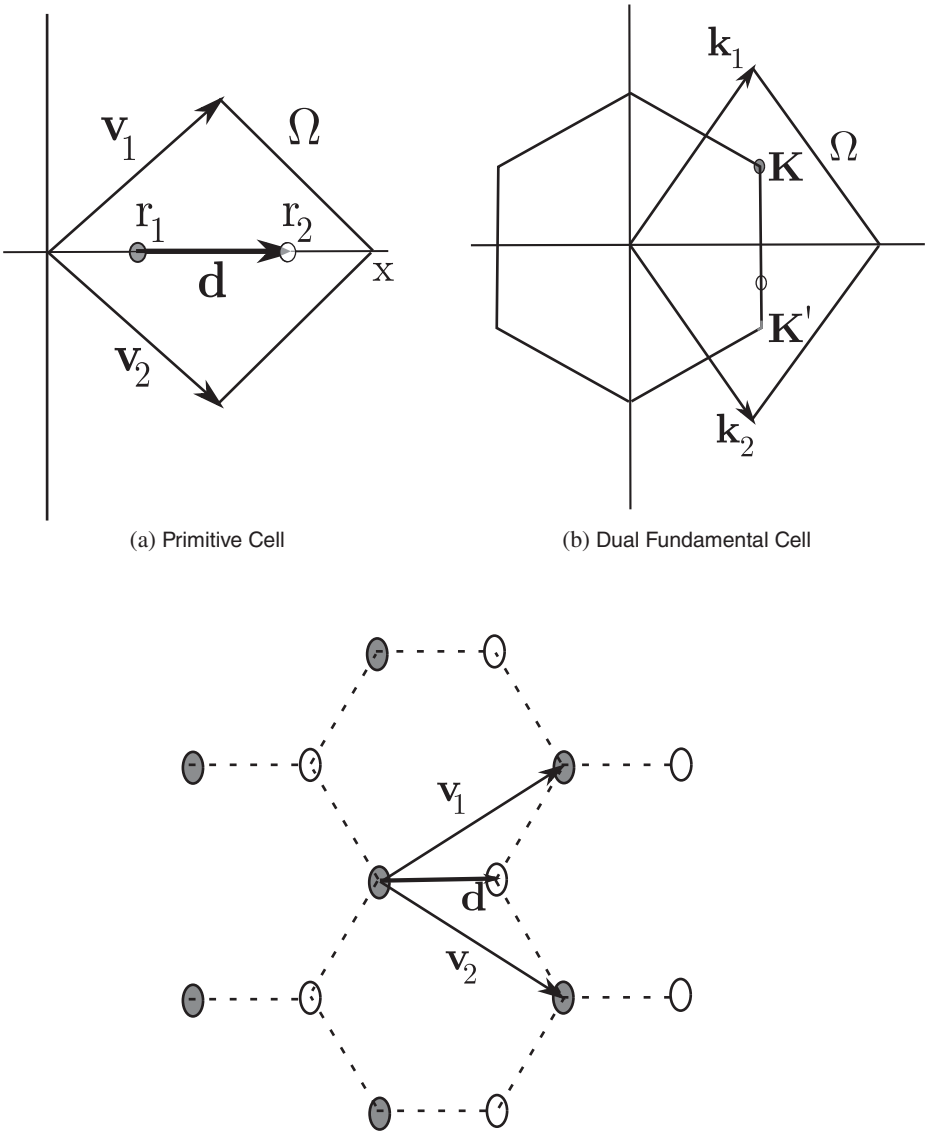

(a) Primitive Cell

(b) Dual Fundamental Cell

(c) Honeycomb Lattice

Figure 1. The primitive cell Ω, and the location of the wells $\mathbf{r}_j$ is shown in (a). The dual fundamental cell Ω' is shown in (b). Also shown is the Brillouin zone (BZ), and its distinguished corners $\mathbf{K}$ and $\mathbf{K}'$. The honeycomb lattice formed from the wells is shown in (c). Strain is introduced by decreasing the horizontal separation between the wells in the honeycomb lattice.

Any other corner of BZ is obtained by rotating $\mathbf{K}$ or $\mathbf{K}'$ by $2\pi/3$ radians. Only two inequivalent corners of the BZ appear in the dual fundamental cell Ω'.

Given the above definitions of the lattice, we define the operator

$$H_0 = -\Delta + \frac{1}{h^2}V,$$

where $V(\mathbf{r})$ is a real, $\mathbb{P}$-periodic function. Via a Floquet–Bloch decomposition, cf. [45], one has that the spectrum of H_0, $\sigma(H_0)$, can be written as

$$\sigma(H_0) = \bigcup_{\mathbf{k}\in\Omega'} \sigma(H_0(\mathbf{k}))$$

where $H_0(\mathbf{k})$ is given by

$$H_0(\mathbf{k}) = -\Delta - 2i\mathbf{k}\cdot\nabla + |\mathbf{k}|^2 + \frac{1}{h^2}V(\mathbf{r}),$$

with $\mathbf{k}$ taking on all values in Ω'. The spectrum $\sigma(H_0(\mathbf{k}))$ is discrete, being composed of some countable number of $\mathbf{k}$ dependent eigenvalues, $\mu_l(\mathbf{k})$, so that we may write

$$\sigma(H_0(\mathbf{k})) = \{\mu_l(\mathbf{k})\}_{l=0}^{\infty}.$$

We define the lth band, B_l, of $\sigma(H_0)$, to be the collection of all eigenvalues $\mu_l(\mathbf{k})$ for $\mathbf{k} \in \Omega'$.

Associated with the eigenvalue, or dispersion relationship, $\mu_l(\mathbf{k})$, one defines the Bloch-mode $\varphi_l(\mathbf{r};\mathbf{k})$ by

$$H_0\varphi_l(\mathbf{r},\mathbf{k}) = \mu_l(\mathbf{k})\varphi_l(\mathbf{r},\mathbf{k}), \tag{2}$$

which implies $\varphi_l(\mathbf{r}+\mathbf{v}_j,\mathbf{k}) = e^{i\mathbf{k}\cdot\mathbf{v}_j}\varphi_l(\mathbf{r},\mathbf{k})$ and $\varphi_l(\mathbf{r},\mathbf{k}+\mathbf{k}_j) = \varphi_l(\mathbf{r},\mathbf{k})$ for all j. Likewise, $\mu_l(\mathbf{k}+\mathbf{k}_j) = \mu_l(\mathbf{k})$ for $j = 1, 2$. Associated with the Bloch-mode is the function $\bar{\varphi}_l(\mathbf{r},\mathbf{k}) = \varphi_l(\mathbf{r},\mathbf{k})e^{-i\mathbf{k}\cdot\mathbf{r}}$, which is an eigenfunction of the operator $H_0(\mathbf{k})$, i.e.

$$H_0(\mathbf{k})\bar{\varphi}_l(\mathbf{r},\mathbf{k}) = \mu_l(\mathbf{k})\bar{\varphi}_l(\mathbf{r},\mathbf{k}). \tag{3}$$

Because of the honeycomb symmetries, as shown in Ref. [13] and rigorously proven in [15], at the vertices of BZ, the two lowest bands, say $\mu_0(\mathbf{k})$ and $\mu_1(\mathbf{k})$, intersect in a conical fashion. This is to say that around $\mathbf{K}$ we have

$$\mu_0(\mathbf{k}) = \tilde{\mu}(\mathbf{K}) - |\bar{\lambda}||\mathbf{k}-\mathbf{K}| + \mathcal{O}(|\mathbf{k}-\mathbf{K}|^2),$$
$$\mu_1(\mathbf{k}) = \tilde{\mu}(\mathbf{K}) + |\bar{\lambda}||\mathbf{k}-\mathbf{K}| + \mathcal{O}(|\mathbf{k}-\mathbf{K}|^2),$$

where $\bar{\lambda}$ is a nonzero complex value that is identical to the parameter $\lambda_\sharp$ in [15]. The effect of this conical intersection is to make the group velocity undefined at the wavenumber $\mathbf{K}$. It is this feature which leads to the most interesting phenomena associated with optical graphene. A similar result holds

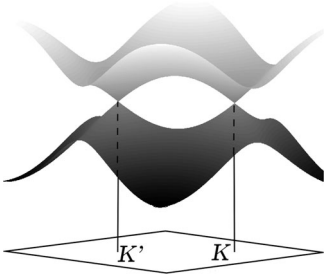

Figure 2. Conical intersections between bands at the two Dirac points **K** and **K**′

around $\mathbf{K}'$. See Figure 2 for reference, and cf. [13] and [15] for more details and examples of honeycomb lattices. We also point out that the results in Ref. [15] hold for lattices which undergo strain as described above. This is explained in greater detail in Section 1.3.

1.2. $\mathcal{PT}$ Symmetry

We now define the notions of $\mathcal{P}$, or spatial inversion, and $\mathcal{T}$, or time-reversal, that we use to define $\mathcal{PT}$ symmetric operators. Following Ref. [20], the action of $\mathcal{P}$ is given by

$$\mathcal{P} : \mathbf{r} \to -\mathbf{r}, \nabla \to -\nabla,$$

and the action of $\mathcal{T}$ is given by

$$\mathcal{T} : i\nabla \to -i\nabla, i \to -i.$$

In order to have $\mathcal{PT}$-symmetry, we must have that $W(\mathbf{r})$ is odd. Given this, it is straightforward to show that $\sigma(H_\vartheta(\mathbf{k}))$, where

$$H_\vartheta(\mathbf{k}) = H_0(\mathbf{k}) + i\vartheta W(\mathbf{r}),$$

is symmetric about the real axis. Thus, simple eigenvalues cannot leave the real axis in $\mathcal{PT}$-symmetric problems. Further, if eigenvalues leave the real axis, or if there is a phase transition, they must either collide, or a degeneracy must be lifted.

Given the degeneracy of the spectrum at the Dirac points, it is a nontrivial question as to whether even small $\mathcal{PT}$ perturbations to H_0 induce phase transitions. To address this issue, in Ref. [37], a perturbation scheme was developed which rigorously established for the two lowest eigenvalues $\mu_0(\mathbf{k};\vartheta)$ and $\mu_1(\mathbf{k};\vartheta)$ of $H_\vartheta(\mathbf{k})$ that

THEOREM 1. *For ϑ sufficiently small, $\mu_0(\mathbf{k};\vartheta)$ and $\mu_1(\mathbf{k};\vartheta)$ are real if and only if $W(\mathbf{r})$ satisfies the orthogonality condition*

$$W_{11} = \int_\Omega W(\mathbf{r})\,|\bar{\varphi}_0(\mathbf{r},\mathbf{K})|^2\,d\mathbf{r} = 0, \tag{4}$$

where $\bar{\varphi}_0$ is defined in (3). We describe those W that satisfy (4) as *real-mass* potentials. In the case that (4) is not satisfied, then we say that W is an *imaginary-mass* potential. As shown in Ref. [37], the difference between these two classes of perturbations comes down to the presence of added symmetries in the problem.

In the case that (4) is not satisfied, a phase transition occurs for $\epsilon \neq 0$, and the Dirac point splits into the two parts

$$\mu_0(\mathbf{K};\vartheta) \sim \mu_0(\mathbf{K}) - i\vartheta\,|W_{11}|, \tag{5}$$

$$\mu_1(\mathbf{K};\vartheta) \sim \mu_0(\mathbf{K}) + i\vartheta\,|W_{11}|. \tag{6}$$

If (4) is satisfied, then it is shown in Ref. [37] that the eigenvalues $\mu_0(\mathbf{K};\vartheta)$ and $\mu_1(\mathbf{K};\vartheta)$ remain real and are given by

$$\mu_0(\mathbf{K};\vartheta) \sim \mu_0(\mathbf{K}) - \vartheta^2\alpha - \vartheta^2\tilde{\Delta}_T, \tag{7}$$

$$\mu_1(\mathbf{K};\vartheta) \sim \mu_0(\mathbf{K}) - \vartheta^2\alpha + \vartheta^2\tilde{\Delta}_T. \tag{8}$$

where α is given by

$$\alpha = \int_\Omega W(\mathbf{r})\bar{\varphi}_0^*(\mathbf{r},\mathbf{K})\,(H_0(\mathbf{K}) - \mu_0(\mathbf{K}))^{-1}\,(1-P_0)W(\mathbf{r})\bar{\varphi}_0(\mathbf{r},\mathbf{K})\,d\mathbf{r}, \tag{9}$$

with P_0 the projection onto the subspace spanned by $\bar{\varphi}_0(\mathbf{r},\mathbf{K})$ and $\bar{\varphi}_1(\mathbf{r},\mathbf{K})$. The detuning parameter, $\tilde{\Delta}_T$, where

$$\Delta_T = \left| \int_\Omega W(\mathbf{r})\bar{\varphi}_0^*(\mathbf{r};\mathbf{K})\,(H_0(\mathbf{K}) - \mu_0(\mathbf{K}))^{-1}\,(1-P_0)W(\mathbf{r})\bar{\varphi}_1(\mathbf{r};\mathbf{K})\,d\mathbf{r} \right|,$$

separates the Dirac points. By splitting the Dirac points, and thus introducing a band gap, the detuning parameter removes the conical intersection between dispersion bands which then allows for a well defined group velocity to be associated with each dispersion band. See Ref. [37] for more details.

1.3. Tight-binding approximations and the strain parameter

By a tight-binding approximation, we mean asymptotic expansions derived in the limit of infinite well depth, or as $h \to 0$, which we call the tight-binding limit. To build these expansions, following the approach in Ref. [11], we define "orbitals" via the eigenvalue problem

$$L_{or}\phi_1^{(or)} = -\Delta\phi_1^{(or)} + \frac{1}{h^2}V_{or}(\mathbf{r})\phi_1^{(or)} = \tilde{E}\phi_1^{(or)}. \tag{10}$$

We define the potential V_{or} to be

$$V_{or}(\mathbf{r}) = V(\mathbf{r}) + (1 - \chi(\mathbf{r})) = V(\mathbf{r}) + \tilde{\delta} V_{or}(\mathbf{r}), \tag{11}$$

where, having chosen an appropriate value $\eta_0 > 0$, we define the function $\chi(\mathbf{r})$ to be smooth, satisfy $0 \leq \chi(\mathbf{r}) \leq 1$, have compact support in $B_A(\mathbf{r}_1, \eta_0)$, and be chosen so that

$$\chi|_{B_A(\mathbf{r}_1, \frac{\eta_0}{2})} = 1.$$

By $B_A(\mathbf{r}_1, \eta_0)$ we mean a ball of radius η_0 around $\mathbf{r}_1$ where distance is measured in terms of the Agmon metric [46] constructed with the honeycomb potential V. We omit the details of this construction for brevity, though see Ref. [12] for more details.

By construction, V_{or} is a one-well potential, i.e. $V_{or}(\mathbf{r}_1) = 0$, but $V_{or}(\mathbf{r}) > 0$ for $\mathbf{r} \neq \mathbf{r}_1$, and therefore a number of theorems become available to us that allow us to approximate solutions to the eigenvalue problem (10). One has that $\phi_1^{(or)}(\mathbf{r}) \in L_2(\mathbb{R}^2)$, and in the tight-binding limit where $h \to 0$, one can show $\phi_1^{(or)}(\mathbf{r})$ is to leading order a Gaussian which decays exponentially fast, cf. [11,47] and the Appendix for details. We can of course repeat all of the above arguments around the second well of $V(\mathbf{r})$ at $\mathbf{r}_2 = \mathbf{r}_1 + \mathbf{d}$, and so we define the second orbital function

$$\phi_2^{(or)}(\mathbf{r}) = \phi_1^{(or)}(\mathbf{r} - \mathbf{d}). \tag{12}$$

We likewise define the functions, which can be thought of as potentials with zero support around either wells,

$$\tilde{\delta} V_1(\mathbf{r}) = \tilde{\delta} V_{or}(\mathbf{r}), \tilde{\delta} V_2(\mathbf{r}) = \tilde{\delta} V_{or}(\mathbf{r} - \mathbf{d}). \tag{13}$$

Therefore, orbitals track the local behavior of wave functions around each well of the potential $V(\mathbf{r})$. In the tight-binding limit, by building expansions of periodically translated orbitals, one can find for the first two bands of (3) the approximations [11]

$$\mu_0(\mathbf{k}) \sim \tilde{E} + c_0^{(tb)} - \epsilon\,|\gamma(\mathbf{k})|\,,$$
$$\mu_1(\mathbf{k}) \sim \tilde{E} + c_0^{(tb)} + \epsilon\,|\gamma(\mathbf{k})|\,,$$

where

$$\gamma(\mathbf{k}) = 1 + \rho\left(e^{-i\mathbf{k}\cdot\mathbf{v}_1} + e^{-i\mathbf{k}\cdot\mathbf{v}_2}\right),$$

$$c_0^{(tb)} = \frac{1}{h^2}\int_{\mathbb{R}^2} \left|\phi_1^{(or)}(\mathbf{r})\right|^2 \tilde{\delta} V_{or}(\mathbf{r}) d\mathbf{r}, \tag{14}$$

and $\epsilon = \mathcal{O}(e^{-1/h}/h^2)$. The parameter ρ is the "strain-parameter," which is explained below in this section. See Equations (A.4) and (A.5) in the Appendix for the tight-binding approximations used to find the dispersion band expansions.

To define the strain parameter ρ, we define the coefficients

$$
\begin{aligned}
c_1^{(tb)} &= \left\langle \phi_1^{(or)}, \phi_2^{(or)} \right\rangle_d, \\
c_2^{(tb)} &= \left\langle \tilde{\delta} V_1 \phi_1^{(or)}, \phi_2^{(or)} \right\rangle_d = \left\langle \tilde{\delta} V_2 \phi_2^{(or)}, \phi_1^{(or)} \right\rangle_d, \\
\rho_1 &= \frac{\left\langle \phi_1^{(or)}, \phi_{2,-\mathbf{v}_k}^{(or)} \right\rangle_d}{c_1^{(tb)}} = \frac{\left\langle \phi_2^{(or)}, \phi_{1,\mathbf{v}_k}^{(or)} \right\rangle_d}{c_1^{(tb)}}, \\
\rho_2 &= \frac{\left\langle \tilde{\delta} V_1 \phi_1^{(or)}, \phi_{2,-\mathbf{v}_k}^{(or)} \right\rangle_d}{c_2^{(tb)}} = \frac{\left\langle \tilde{\delta} V_2 \phi_2^{(or)}, \phi_{1,\mathbf{v}_k}^{(or)} \right\rangle_d}{c_2^{(tb)}},
\end{aligned}
$$

where $\phi_{j,\mathbf{v}_k}^{(or)}(\mathbf{r}) = \phi_j^{(or)}(\mathbf{r} - \mathbf{v}_k)$, $k = 1, 2$. We have taken, via symmetry arguments, ρ_1 and ρ_2 to be independent of the choice of $\mathbf{v}_1$ or $\mathbf{v}_2$. Letting

$$
C^{(tb)} = c_0^{(tb)} c_1^{(tb)} - c_2^{(tb)}, \tag{15}
$$

where we note that $C^{(tb)} = \mathcal{O}(\epsilon)$, we define the strain, or deformation, parameter ρ via the equation

$$
\rho = \frac{c_0^{(tb)} c_1^{(tb)} \rho_1 - c_2^{(tb)} \rho_2}{C^{(tb)}}. \tag{16}
$$

This parameter tracks strain since as the length of the separation vector $\mathbf{d}$ changes, all values in (16) change as well. For unstrained lattices, $\rho = 1$.

As a result of strain, the location of the Dirac points changes. The formula relating the position of the Dirac points to strain in the lattice was derived in Ref. [11] and is given by

$$
\mathbf{K}_\rho = \frac{2}{\ell} \begin{pmatrix} 0 \\ \pi - \cos^{-1}\left(\frac{1}{2\rho}\right) \end{pmatrix}, \mathbf{K}_\rho^{'} = -\mathbf{K}_\rho. \tag{17}
$$

This shows under significant strain, i.e. when $\rho < 1/2$, the Dirac points are no longer present, which implies the lowest dispersion bands separate. This strain induced band gap plays a crucial role in the analysis of Section 2.

1.4. Notational conventions

In the text, we use two different inner products. By $\langle \cdot, \cdot \rangle_d$ we mean the $L_2(\mathbb{R}^2)$ inner product, or for $f(\mathbf{r})$ and $q(\mathbf{r})$

$$
\langle f, q \rangle_d = \int_{\mathbb{R}^2} f(\mathbf{r}) q^*(\mathbf{r}) d\mathbf{r}.
$$

By $\langle \cdot, \cdot \rangle_p$ we mean the $L^2(\Omega)$ inner product where

$$\langle f, q \rangle_p = \int_\Omega f(\mathbf{r}) q^*(\mathbf{r}) d\mathbf{r}.$$

Likewise, $||\cdot||_{2,p}$ refers to the $L^2(\Omega)$ norm.

2. Discrete and dirac systems for imaginary-mass potentials

The tight-binding approximation is formed by approximating the solution $u(\mathbf{r}, z)$ to (1) via the expansion

$$u \sim \sqrt{\frac{\epsilon}{g}} \left(\sum_{\mathbf{v} \in \mathbb{P}} \left(a_\mathbf{v}(\epsilon z) \phi_1^{(or)}(\mathbf{r} - \mathbf{v}) + b_\mathbf{v}(\epsilon z) \phi_2^{(or)}(\mathbf{r} - \mathbf{v}) \right) e^{i\mathbf{k}\cdot\mathbf{v}} \right) e^{-i(\tilde{E} + c_0^{(tb)})z},$$

where the constant g is given by

$$g = \int_{\mathbb{R}^2} \phi_1^4 d\mathbf{r}.$$

We then define $\phi_{1,\mathbf{v}} = \phi_1^{(or)}(\mathbf{r} - \mathbf{v})$, $\phi_{2,\mathbf{v}} = \phi_2^{(or)}(\mathbf{r} - \mathbf{v})$, and

$$\tilde{\delta} V_{s,\mathbf{v}} = \tilde{\delta} V_s(\mathbf{r} - \mathbf{v}), \tilde{s} = 1, 2.$$

Again, please see Equations (11, 12), and (13) for reference. The term $c_0^{(tb)}$ is given by (14) and $\tilde{E}$ is defined in (10).

By inserting the expansion for u and factoring out the fast phase $e^{-i(\tilde{E} + c_0^{(tb)})z}$, we get the expression

$$\begin{aligned} & i\epsilon \sum_\mathbf{v} \left(\dot{a}_\mathbf{v} \phi_{1,\mathbf{v}} + \dot{b}_\mathbf{v} \phi_{2,\mathbf{v}} \right) e^{i\mathbf{k}\cdot\mathbf{v}} + c_0^{(tb)} \sum_\mathbf{v} \left(a_\mathbf{v} \phi_{1,\mathbf{v}} + b_\mathbf{v} \phi_{2,\mathbf{v}} \right) e^{i\mathbf{k}\cdot\mathbf{v}} \\ & -\frac{1}{h^2} \sum_\mathbf{v} \left(a_\mathbf{v} \tilde{\delta} V_{1,\mathbf{v}} \phi_{1,\mathbf{v}} + b_\mathbf{v} \tilde{\delta} V_{2,\mathbf{v}} \phi_{2,\mathbf{v}} \right) e^{i\mathbf{k}\cdot\mathbf{v}} + i\vartheta W(\mathbf{r}) \sum_\mathbf{v} \left(a_\mathbf{v} \phi_{1,\mathbf{v}} + b_\mathbf{v} \phi_{2,\mathbf{v}} \right) e^{i\mathbf{k}\cdot\mathbf{v}} \\ & + \sigma \frac{\epsilon}{g} \left| \sum_\mathbf{v} \left(a_\mathbf{v} \phi_{1,\mathbf{v}} + b_\mathbf{v} \phi_{2,\mathbf{v}} \right) e^{i\mathbf{k}\cdot\mathbf{v}} \right|^2 \sum_\mathbf{v} \left(a_\mathbf{v} \phi_{1,\mathbf{v}} + b_\mathbf{v} \phi_{2,\mathbf{v}} \right) e^{i\mathbf{k}\cdot\mathbf{v}} = 0, \end{aligned}$$

where $\dot{a} = \partial_Z a$ and $\dot{b} = \partial_Z b$, with $Z = \epsilon z$. We now take inner products with respect to both $\phi_{1,\mathbf{p}}$ and $\phi_{2,\mathbf{p}}$. As shown in Ref. [11, 12], we have the following asymptotic balances

$$\begin{aligned} \left\langle \phi_{1,\mathbf{v}}, \phi_{1,\mathbf{v}} \right\rangle_d = \left\langle \phi_{2,\mathbf{v}}, \phi_{2,\mathbf{v}} \right\rangle_d = \langle \phi_1, \phi_1 \rangle_d = 1, \\ \left\langle \phi_{1,\mathbf{p}}, \phi_{2,\mathbf{v}} \right\rangle_d \ll \langle \phi_2, \phi_1 \rangle_d = \mathcal{O}(\epsilon), \\ \frac{1}{h^2} \left\langle \tilde{\delta} V_{1,\mathbf{v}} \phi_{1,\mathbf{v}}, \phi_{2,\mathbf{v}} \right\rangle_d = \frac{1}{h^2} \left\langle \tilde{\delta} V_{2,\mathbf{v}} \phi_{2,\mathbf{v}}, \phi_{1,\mathbf{v}} \right\rangle_d = \mathcal{O}(\epsilon), \end{aligned}$$

where $\mathbf{p} \in \mathbb{P}$. For the inner product with respect to $\phi_{1,\mathbf{p}}$, counting only up to nearest neighbor interactions, using (15) and (16), and the substitutions

$$a_{\mathbf{p}} = \tilde{a}_{\mathbf{p}} e^{ic_0^{(tb)} Z/\epsilon},\ b_{\mathbf{p}} = \tilde{b}_{\mathbf{p}} e^{ic_0^{(tb)} Z/\epsilon},$$

we get to leading order the equation

$$\begin{aligned} &i\epsilon\partial_Z a_{\mathbf{p}} + C^{(tb)} b_{\mathbf{p}} + C^{(tb)}\rho(b_{\mathbf{p}-\mathbf{v}_1} e^{-i\mathbf{k}\cdot\mathbf{v}_1} + b_{\mathbf{p}-\mathbf{v}_2} e^{-i\mathbf{k}\cdot\mathbf{v}_2}) \\ &\quad + i\left(\tilde{W}_{01} a_{\mathbf{p}} + \tilde{W}_1 b_{\mathbf{p}} + \tilde{W}_2(b_{\mathbf{p}-\mathbf{v}_1} e^{-i\mathbf{k}\cdot\mathbf{v}_1} + b_{\mathbf{p}-\mathbf{v}_2} e^{-i\mathbf{k}\cdot\mathbf{v}_2})\right) + \sigma\epsilon|a_{\mathbf{p}}|^2 a_{\mathbf{p}} = 0, \end{aligned}$$

where we have dropped the tildes on $a_{\mathbf{p}}$ and $b_{\mathbf{p}}$ and

$$\begin{aligned} \tilde{W}_{01} &= \vartheta \int_{\mathbb{R}^2} W(\mathbf{r})\phi_1^2(\mathbf{r})d\mathbf{r}, \\ \tilde{W}_1 &= \vartheta \int_{\mathbb{R}^2} W(\mathbf{r})\phi_1(\mathbf{r})\phi_2(\mathbf{r})d\mathbf{r}, \\ \tilde{W}_2 &= \vartheta \int_{\mathbb{R}^2} W(\mathbf{r})\phi_1(\mathbf{r})\phi_{2,-\mathbf{v}_1}(\mathbf{r})d\mathbf{r} = \vartheta \int_{\mathbb{R}^2} W(\mathbf{r})\phi_1(\mathbf{r})\phi_{2,-\mathbf{v}_2}(\mathbf{r})d\mathbf{r}, \end{aligned}$$

with $j = 1, 2$. Note, by $\phi_j(\mathbf{r})$, we mean $\phi_j^{(or)}(\mathbf{r})$. We have also used the fact that to leading order each ϕ_j is real; see the Appendix for details. Likewise, by taking an inner product with respect to $\phi_{2,\mathbf{p}}$, we get

$$\begin{aligned} &i\epsilon\partial_Z b_{\mathbf{p}} + C^{(tb)} a_{\mathbf{p}} + C^{(tb)}\rho(a_{\mathbf{p}+\mathbf{v}_1} e^{i\mathbf{k}\cdot\mathbf{v}_1} + a_{\mathbf{p}+\mathbf{v}_2} e^{i\mathbf{k}\cdot\mathbf{v}_2}) \\ &\quad + i\left(\tilde{W}_{02} b_{\mathbf{p}} + \tilde{W}_1 a_{\mathbf{p}} + \tilde{W}_2(a_{\mathbf{p}+\mathbf{v}_1} e^{i\mathbf{k}\cdot\mathbf{v}_1} + a_{\mathbf{p}+\mathbf{v}_2} e^{i\mathbf{k}\cdot\mathbf{v}_2})\right) + \sigma\epsilon|b_{\mathbf{p}}|^2 b_{\mathbf{p}} = 0, \end{aligned}$$

where

$$\tilde{W}_{02} = \vartheta \int_{\mathbb{R}^2} W(\mathbf{r})\phi_2^2(\mathbf{r})d\mathbf{r}.$$

We now analyze the terms $\tilde{W}_{01}$ and $\tilde{W}_{02}$. In the tight-binding limit, the function $\phi_1(\mathbf{r})$ limits to a function with compact support centered around $\mathbf{r}_1$; see the Appendix for details. In order for the imaginary-mass condition to have meaning in this case, we must suppose that $W(\mathbf{r})$ has nontrivial support at $\mathbf{r}_1$. An example of a valid choice of $W(\mathbf{r})$ that satisfies this requirement is given by

$$W(\mathbf{r}) = \frac{1}{2}\left(\sin(\mathbf{k}_1 \cdot \mathbf{r}) + \sin(\mathbf{k}_2 \cdot \mathbf{r})\right). \tag{18}$$

A plot of this function is in Figure 3 where one can see that $W(\mathbf{r})$ is $\mathcal{O}(1)$ around each well. Therefore, we take $\tilde{W}_{01} = \mathcal{O}(\vartheta)$. Likewise, for $\tilde{W}_{02}$, if we first shift

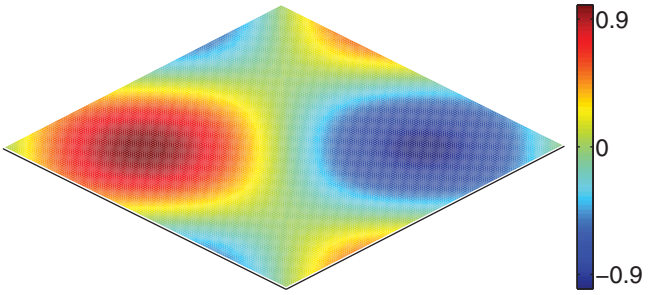

Figure 3. Plot of (18). Note that $W(\mathbf{r})$ is $\mathcal{O}(1)$ over each well $\mathbf{r}_1$ and $\mathbf{r}_2$.

to the left by $\mathbf{v}_{12} = \mathbf{v}_1 + \mathbf{v}_2$, and use the fact that $2\mathbf{r}_1 + \mathbf{d} = \mathbf{v}_{12}$, then we get that

$$\begin{aligned}\tilde{W}_{02} &= \vartheta \int_{\mathbb{R}^2} W(\mathbf{r})(\phi^{(or)}(\mathbf{r} + \mathbf{v}_{12} - \mathbf{r}_1 - \mathbf{d}))^2 d\mathbf{r}, \\ &= \vartheta \int_{\mathbb{R}^2} W(\mathbf{r})(\phi^{(or)}(\mathbf{r} + \mathbf{r}_1))^2 d\mathbf{r}, \\ &= -\vartheta \int_{\mathbb{R}^2} W(\mathbf{r})(\phi^{(or)}(\mathbf{r} - \mathbf{r}_1))^2 d\mathbf{r},\end{aligned}$$

so that $\tilde{W}_{02} = -\tilde{W}_{01}$.

Noting again the convention that $\phi_1(\mathbf{r}) = \phi_1^{(or)}(\mathbf{r}) = \phi^{(or)}(\mathbf{r} - \mathbf{r}_1)$, to leading order $\phi^{(or)}(\mathbf{r})$ is an even function since it is well approximated by the ground state eigenfunction of a two-dimensional harmonic oscillator problem; see the Appendix for details. This implies

$$\begin{aligned}\tilde{W}_1 &= \vartheta \int_{\mathbb{R}^2} W(\mathbf{r})\phi_1(\mathbf{r})\phi_1(\mathbf{r} - \mathbf{d}) d\mathbf{r}, \\ &= \vartheta \int_{\mathbb{R}^2} W(\mathbf{r})\phi_1(\mathbf{r} + \mathbf{v}_{12})\phi_1(\mathbf{r} + \mathbf{v}_{12} - \mathbf{d}) d\mathbf{r}, \\ &= \vartheta \int_{\mathbb{R}^2} W(\mathbf{r})\phi^{(or)}(\mathbf{r} + \mathbf{r}_1 + \mathbf{d})\phi^{(or)}(\mathbf{r} + \mathbf{r}_1) d\mathbf{r}, \\ &\sim -\vartheta \int_{\mathbb{R}^2} W(\mathbf{r})\phi^{(or)}(\mathbf{r} - \mathbf{r}_1 - \mathbf{d})\phi^{(or)}(\mathbf{r} - \mathbf{r}_1) d\mathbf{r}, \\ &\sim -\tilde{W}_1,\end{aligned}$$

which implies $|\tilde{W}_1| \ll \vartheta$. Likewise, we have that

$$\tilde{W}_2 = \vartheta \int_{\mathbb{R}^2} W(\mathbf{r})\phi_1(\mathbf{r})\phi_1(\mathbf{r} - \mathbf{d} + \mathbf{v}_j) d\mathbf{r},$$

$$
\begin{aligned}
&= \vartheta \int_{\mathbb{R}^2} W(\mathbf{r})\phi_1(\mathbf{r}+\mathbf{v}_{12})\phi_1(\mathbf{r}+\mathbf{v}_{12}-\mathbf{d}+\mathbf{v}_j)d\mathbf{r},\\
&= \vartheta \int_{\mathbb{R}^2} W(\mathbf{r})\phi^{(or)}(\mathbf{r}+\mathbf{r}_1+\mathbf{d})\phi^{(or)}(\mathbf{r}+\mathbf{r}_1+\mathbf{v}_j)d\mathbf{r},\\
&\sim -\vartheta \int_{\mathbb{R}^2} W(\mathbf{r})\phi^{(or)}(\mathbf{r}-\mathbf{r}_1-\mathbf{d})\phi^{(or)}(\mathbf{r}-\mathbf{r}_1-\mathbf{v}_j)d\mathbf{r},\\
&\sim -\tilde{W}_2,
\end{aligned}
$$

and so $|\tilde{W}_2| \ll \vartheta$.

The terms $\tilde{W}_1$ and $\tilde{W}_2$ are asymptotically negligible compared to $\tilde{W}_{01}$ and $\tilde{W}_{02}$, and so we ignore them. Then, dividing by $C^{(tb)}$, we get the equation for $a_{\mathbf{p}}$

$$
i\,\partial_Z a_{\mathbf{p}} + i\,\frac{\tilde{W}_{01}}{\epsilon}a_{\mathbf{p}} + (\mathcal{L}_- b)_{\mathbf{p}} + \sigma|a_{\mathbf{p}}|^2 a_{\mathbf{p}} = 0, \tag{19}
$$

where

$$
(\mathcal{L}_- b)_{\mathbf{p}} = b_{\mathbf{p}} + \rho(b_{\mathbf{p}-\mathbf{v}_1}e^{-i\mathbf{k}\cdot\mathbf{v}_1} + b_{\mathbf{p}-\mathbf{v}_2}e^{-i\mathbf{k}\cdot\mathbf{v}_2}),
$$

and where we have divided $\tilde{W}_{01}$ by $C^{(tb)}$ so that it is now a $\mathcal{O}(\vartheta/\epsilon)$ value. While we have left ϑ free up to this point, we assume that

$$
\vartheta/\epsilon \ll 1,
$$

but that this ratio is significantly larger than any of the next-nearest neighbor effects we have removed using our tight-binding approximation.

An identical argument then gives us

$$
i\,\partial_Z b_{\mathbf{p}} - i\,\frac{\tilde{W}_{01}}{\epsilon}b_{\mathbf{p}} + (\mathcal{L}_+ a)_{\mathbf{p}} + \sigma|b_{\mathbf{p}}|^2 b_{\mathbf{p}} = 0, \tag{20}
$$

where

$$
(\mathcal{L}_+ a)_{\mathbf{p}} = a_{\mathbf{p}} + \rho(a_{\mathbf{p}+\mathbf{v}_1}e^{i\mathbf{k}\cdot\mathbf{v}_1} + a_{\mathbf{p}+\mathbf{v}_2}e^{i\mathbf{k}\cdot\mathbf{v}_2}).
$$

For $\mathbf{p} = n\mathbf{v}_1 + m\mathbf{v}_2$, if we let $\sigma = 0$, and if we then suppose that

$$
a_{\mathbf{p}}(Z) = a_0 e^{i(n\theta_x + m\theta_y - \omega Z)},\ b_{\mathbf{p}}(Z) = b_0 e^{i(n\theta_x + m\theta_y - \omega Z)},
$$

we find the dispersion relationship of the discrete system

$$
\omega = \pm\sqrt{-\tilde{W}_{01}^2/\epsilon^2 + \psi(\tilde{\theta}_1, \tilde{\theta}_2)},
$$

where

$$
\psi(\tilde{\theta}_1, \tilde{\theta}_2) = 1 + 2\rho(\cos(\tilde{\theta}_1) + \cos(\tilde{\theta}_2)) + 2\rho^2(1 + \cos(\tilde{\theta}_1 - \tilde{\theta}_2)),
$$

and where

$$
\tilde{\theta}_1 = \mathbf{k}\cdot\mathbf{v}_1 + \theta_x,\ \tilde{\theta}_2 = \mathbf{k}\cdot\mathbf{v}_2 + \theta_y.
$$

Thus, to prevent a phase transition, we must assume that

$$\psi(\tilde{\theta}_1, \tilde{\theta}_2) \geq \frac{\tilde{W}_{01}^2}{\epsilon^2}.$$

It is straightforward to show that $\psi(\tilde{\theta}_1, \tilde{\theta}_2) \geq 0$, and that if $\rho \geq 1/2$, then $\psi(\tilde{\theta}_1, \tilde{\theta}_2)$ has a zero. Therefore, we must have a phase transition if $\tilde{W}_{01} \neq 0$. However, for $\rho < 1/2$ we get

$$\min\{\psi\} = (1 - 2\rho)^2,$$

and thus if $|\tilde{W}_{01}| < \epsilon(1 - 2\rho)$, then there is no phase transition. This shows how significant strain prevents phase transitions. We emphasize that the role strain plays in preventing phase transitions, and the derivation of the linear tight-binding approximation, has appeared previously in Refs. [34,35]. We have included the derivation and results above for completeness of this text and to elaborate on mathematical details not explicitly included in the previous works.

We note that we have also derived the equivalent real-mass condition $\tilde{W}_{01} = 0$. In fact, we see that

$$\begin{aligned}\tilde{W}_{01} &= \int_\Omega d\mathbf{r} W(\mathbf{r}) \sum_{\mathbf{v}} \left(\phi_{1,\mathbf{v}}^{(or)}(\mathbf{r})\right)^2 \\ &\sim \int_\Omega d\mathbf{r} W(\mathbf{r}) \left|\tilde{\varphi}(\mathbf{r}; \mathbf{K})\right|^2,\end{aligned}$$

so that to leading order $\tilde{W}_{01} = 0$ is in fact equivalent to the real-mass condition. We see from this argument that any effect of a real-mass potential must appear at higher orders than what the tight-binding argument used above can resolve. This issue is dealt with in Section 3.

2.1. The continuum limit and nonlocal nonlinear wave equations

As the only way in which we can avoid a phase transition for imaginary mass potentials is to have a gap between bands, following Ref. [38], we introduce the parameter $\beta = 2\rho - 1$, the slow variables

$$\mathbf{R} = (X, Y) = \epsilon\mathbf{r},\ \tilde{Z} = \epsilon Z,$$

and the parameter $\kappa = |\beta|\epsilon$. Taking a continuum limit in (19) and (20), where we let

$$a_{\mathbf{p}+\mathbf{v}} = \sqrt{\epsilon}(\tilde{a} + \epsilon\mathbf{v} \cdot \nabla_{\mathbf{R}}\tilde{a} + \cdots),\ b_{\mathbf{p}+\mathbf{v}} = \sqrt{\epsilon}(\tilde{b} + \epsilon\mathbf{v} \cdot \nabla_{\mathbf{R}}\tilde{b} + \cdots),$$

and repeating the computations found in section 6 of Ref. [38] then gives us, after dropping tildes, the Dirac-like system

$$\begin{aligned} i\partial_{\tilde{Z}}a + i\tilde{W}a + (1 - \kappa\epsilon)\mathcal{F}b + \kappa b + \sigma|a|^2 a &= 0 \\ i\partial_{\tilde{Z}}b - i\tilde{W}b + (1 - \kappa\epsilon)\mathcal{F}^\dagger a + \kappa a + \sigma|b|^2 b &= 0, \end{aligned}$$

where $\tilde{W} = \tilde{W}_{01}/\epsilon^2$,

$$\mathcal{F} = \partial_X - \frac{\epsilon}{2}\Delta + \frac{\epsilon^2}{6}\left(\partial_X^3 + \partial_Y^3 + 3\partial_X\partial_Y^2\right),$$

and $\mathcal{F}^\dagger$ denotes the adjoint of $\mathcal{F}$. We emphasize that we take the amplitude to be small and the envelope to be wide in the continuum limit, and it is this requirement which allows us to maintain the localization in wave number around the Dirac point.

At this point, we suppose that ϵ and β are small. Further, we readily see that the dispersion relationship of this system is given by

$$\omega = \pm\sqrt{\left|\kappa + (1-\kappa\epsilon)\hat{\mathcal{F}}\right|^2 - \tilde{W}^2},$$

where $\hat{\mathcal{F}}$ is the Fourier transform or symbol of $\mathcal{F}$. The real part of $\kappa + (1-\kappa\epsilon)\hat{\mathcal{F}}$ is given by

$$\mathrm{Re}(\kappa + (1-\kappa\epsilon)\hat{\mathcal{F}}) = \kappa + \frac{\epsilon|\tilde{\mathbf{k}}|^2}{2}(1-\kappa\epsilon).$$

This is positive for all wave numbers $\tilde{\mathbf{k}}$ if $\kappa\epsilon = |\beta|\epsilon^2 < 1$, which we take to be so. Therefore, we see that we can prevent phase transitions when

$$|\tilde{W}| \leq \kappa,$$

which is effectively the same condition as above in the discrete system.

If $\kappa \ll 1$, we can rewrite the nonlinear Dirac equation as

$$i\partial_{\tilde{Z}}a + \partial_X b = \mathcal{G}_1, i\partial_{\tilde{Z}}b - \partial_X a = \mathcal{G}_2,$$

where $\mathcal{G}_j$ are asymptotically small; see Ref. [38] for more explicit representations of $\mathcal{G}_j$. By introducing the traveling coordinates

$$\xi = X - \tilde{Z}, \eta = X + \tilde{Z},$$

and the variables

$$\bar{a} = -ia + b, \bar{b} = ia + b,$$

we can transform the nonlinear Dirac equation into

$$\partial_\xi \bar{a} = \frac{1}{2}\left(\mathcal{G}_1 + i\mathcal{G}_2\right), \partial_\eta \bar{b} = \frac{1}{2}\left(\mathcal{G}_1 - i\mathcal{G}_2\right).$$

To have the classic wave equation in characteristic coordinates at leading order, we look at the modified system

$$\partial_\eta\partial_\xi \bar{a} = \frac{1}{2}\partial_\eta\left(\mathcal{G}_1 + i\mathcal{G}_2\right), \partial_\xi\partial_\eta \bar{b} = \frac{1}{2}\partial_\xi\left(\mathcal{G}_1 - i\mathcal{G}_2\right).$$

We then suppose that

$$\bar{a} = \sqrt{\delta}\left(\bar{a}_0(\eta, Y, \delta\tilde{Z}) + \bar{a}_1(\xi, \eta, Y, \delta\tilde{Z})\right)$$
$$\bar{b} = \sqrt{\delta}\left(\bar{b}_0(\xi, Y, \delta\tilde{Z}) + \bar{b}_1(\xi, \eta, Y, \delta\tilde{Z})\right),$$

where we assume that $\bar{a}_1$ and $\bar{b}_1$ are both $\mathcal{O}(\delta)$. The above equations become

$$\partial_\eta\partial_\xi\bar{a}_1 = \frac{1}{2}\left(\partial_\eta\left(\frac{\mathcal{G}_1 + i\mathcal{G}_2}{\sqrt{\delta}}\right) + \delta\partial_\eta\partial_{\bar{Z}}\bar{a}_0 + \delta\partial_\eta\partial_{\bar{Z}}\bar{a}_1\right)$$
$$\partial_\xi\partial_\eta\bar{b}_1 = \frac{1}{2}\left(\partial_\xi\left(\frac{\mathcal{G}_1 - i\mathcal{G}_2}{\sqrt{\delta}}\right) - \delta\partial_\xi\partial_{\bar{Z}}\bar{b}_0 - \delta\partial_\xi\partial_{\bar{Z}}\bar{b}_1\right),$$

where $\bar{Z} = \delta\tilde{Z}$. We note that secular terms for the $\bar{a}_1$ equation are those terms that depend on η only and vice versa for the $\bar{b}_1$ equation.

We then get for the unidirectional envelope $\bar{a}_0$ the equation

$$\frac{1}{\delta}(\kappa^2 - \tilde{W}^2)\bar{a}_0 + \frac{\epsilon\kappa}{2\delta}\left(\partial_\eta^2 - \partial_Y^2\right)\bar{a}_0 + \frac{\epsilon^2}{\delta}\mathcal{M}(\eta)\bar{a}_0 - \frac{i\sigma}{4}\partial_\eta\left(|\bar{a}_0|^2\bar{a}_0\right) + \partial_\eta\partial_{\bar{Z}}\bar{a}_0 = 0,$$

where

$$\mathcal{M}(\eta) = -\frac{1}{24}\partial_\eta^4 + \frac{1}{8}\partial_Y^4 - \frac{1}{6}\partial_Y^3\partial_\eta - \frac{1}{4}\partial_\eta^2\partial_Y^2.$$

For $\bar{b}_0$, we get

$$\frac{1}{\delta}(\kappa^2 - \tilde{W}^2)\bar{b}_0 + \frac{\epsilon\kappa}{2\delta}\left(\partial_\xi^2 - \partial_Y^2\right)\bar{b}_0 + \frac{\epsilon^2}{\delta}\mathcal{M}(\xi)\bar{b}_0 + \frac{i\sigma}{4}\partial_\xi\left(|\bar{b}_0|^2\bar{b}_0\right) - \partial_\xi\partial_{\bar{Z}}\bar{b}_0 = 0,$$

where $\mathcal{M}(\xi)$ is the same as the operator $\mathcal{M}(\eta)$ with η replaced by ξ. In either the $\bar{a}_0$ or $\bar{b}_0$ equations, we see for $|\tilde{W}| \ll \kappa$, so that the $\mathcal{PT}$ perturbation is a relatively higher order effect, we obtain equations consistent with those in [38]. We see new equations are found by taking the balance $|\tilde{W}| \lesssim \kappa$, $\epsilon \sim \kappa$, and $\delta \sim \epsilon^2$, which gives the equation

$$\frac{1}{2}\left(\partial_\eta^2 - \partial_Y^2\right)\bar{a}_0 + \mathcal{M}(\eta)\bar{a}_0 - \frac{i\sigma}{4}\partial_\eta\left(|\bar{a}_0|^2\bar{a}_0\right) + \partial_\eta\partial_{\bar{Z}}\bar{a}_0 = 0. \tag{21}$$

The equivalent version of this equation in [38] is given by

$$\bar{a}_0 + \frac{1}{2}\left(\partial_\eta^2 - \partial_Y^2\right)\bar{a}_0 + \mathcal{M}(\eta)\bar{a}_0 - \frac{i\sigma}{4}\partial_\eta\left(|\bar{a}_0|^2\bar{a}_0\right) + \partial_\eta\partial_{\bar{Z}}\bar{a}_0 = 0. \tag{22}$$

We could also take the balance $|\tilde{W}| \sim \kappa$, $\epsilon\kappa \ll \delta$, and $\epsilon^2 \ll \delta$ to get the local equation

$$-\frac{i\sigma}{4}|\bar{a}_0|^2\bar{a}_0 + \partial_{\bar{Z}}\bar{a}_0 = \tilde{c}(\bar{Z}), \tag{23}$$

where $\tilde{c}(\bar{Z})$ is an arbitrary function. The equivalent version of this equation in Ref. [38] is given by

$$\bar{a}_0 - \frac{i\sigma}{4}\partial_\eta\left(|\bar{a}_0|^2\bar{a}_0\right) + \partial_{\bar{Z}}\partial_\eta\bar{a}_0 = 0, \tag{24}$$

Therefore, we see that the general effect of the $\mathcal{PT}$ perturbation is to localize the nonlinear wave equations derived in Ref. [38]. A striking way to see this is by comparing the one-dimensional reductions of (21) and (22). These one-dimensional reductions are obtained by ignoring variations in Y. We readily see that the reduced version of (21) can be localized, i.e. the problem can be integrated in η once, and a local equation is obtained. This is not the case for the 1+1 version of (22). Therefore, the $\mathcal{PT}$ perturbation reduces the degree of nonlocality compared to the unperturbed case. Likewise, (23) is a local equation while (24) is nonlocal; this further shows the localizing effect of the $\mathcal{PT}$ perturbation.

2.2. *Semilocalized gap solitons*

Following the discussion above, in (21), we see that by looking for one-dimensional profiles by ignoring variations in the y-direction, (21) reduces to the third order NLS type equation

$$\partial_\eta\bar{a}_0 - \frac{1}{24}\partial_\eta^3\bar{a}_0 - \frac{i\sigma}{4}|\bar{a}_0|^2\bar{a}_0 + \partial_{\bar{Z}}\bar{a}_0 = \hat{c},$$

where $\hat{c}$ is a constant. If we look for localized solutions of the above equation, we then take $\hat{c} = 0$. This equation is equivalent to an NLS equation with higher order dispersion studied in Refs. [48] and [49]. In Ref. [48], families of multihumped solitons were found, and in Ref. [49] the stability of these localized profiles was studied numerically. Ultimately, Ref. [49] described these profiles as semistable, which is to say certain classes of perturbations destabilize these solitons while others do not significantly affect the structure of the localized profile. In the current context, we describe these modes as semilocalized gap solitons since they are nonlinear modes found at a wave-number, i.e. $\mathbf{k} = \mathbf{K}$, that is now in the strain induced band-gap.

Motivated by the above considerations, we now examine the behavior of the one-dimensional solitons found in Refs. [48] and [49] as solutions to (21). In order to compare to the work in Ref. [49], we introduce the following coordinate changes

$$\zeta = \eta - \frac{5}{6}\bar{Z}, \tilde{\zeta} = \zeta/L_\zeta, \tilde{y} = Y/L_y, \tilde{z} = \bar{Z}/T, \tilde{a} = \mathcal{A}\bar{a}_0,$$

where we choose

$$L_\eta = \frac{1}{3^{1/4}2}, L_y = \frac{1}{2}, T = 3^{1/4}, \mathcal{A} = \frac{2}{3^{1/8}},$$

so that (21) becomes, after dropping tildes,

$$\partial_{z\zeta} a - \frac{1}{3}\partial_\zeta^2 a - \partial_y^2 a - \partial_\zeta^4 a + \partial_y^4 a - \hat{c}_1 \partial_y^3 \partial_\zeta a - \hat{c}_2 \partial_y^2 \partial_\zeta^2 a - i\sigma \partial_\zeta \left(|a|^2 a\right) = 0.$$

Here, $\hat{c}_1 = 32(48)^{-3/4}$ and $\hat{c}_2 = 24(48)^{-1/2}$. Following this with the coordinate transformation

$$a(\zeta, y, z) = (\nu + 1/3)^{3/4}\, \bar{a}(\bar{\zeta}, y, z) e^{i(\nu/3+\lambda+2/27)z}$$

where

$$\bar{\zeta} = (\nu + 1/3)^{1/2} (\zeta - \nu z),$$

we then get, dropping the bars on $\bar{a}$ and $\bar{\zeta}$, the equation

$$\begin{aligned} \partial_z a = {} & (\nu + 1/3)^{3/2} \left(\partial_\zeta a + \partial_\zeta^3 a\right) - i(\lambda + \nu/3 + 2/27)a \\ & + (\nu + 1/3)^{-1/2} \partial_\zeta^{-1} \left(\partial_y^2 a - \partial_y^4 a\right) + \hat{c}_1 \partial_y^3 a + \hat{c}_2 (\nu + 1/3)^{1/2} \partial_\zeta \partial_y^2 a \\ & + i\sigma (\nu + 1/3)^{3/2} |a|^2 a \end{aligned} \tag{25}$$

The one-dimensional reduction of this equation is

$$\partial_z a = (\nu + 1/3)^{3/2} \left(\partial_\zeta a + \partial_\zeta^3 a - i(\nu + 1/3)^{-3/2} (\lambda + \nu/3 + 2/27)a + i\sigma |a|^2 a\right).$$

Following [49], we choose λ so that it solves

$$\left(\nu + \frac{1}{3}\right)^{-3/2} \left(\lambda + \frac{\nu}{3} + \frac{2}{27}\right) = .8619,$$

so that we are looking at the first family, cf. [49], of two-pulse solitons. We take $\nu = 1$ and $\sigma = 1$. We introduce a random complex perturbation to the one-dimensional soliton solution which typically looks like the plot in Figure 4a. As seen in Figures 4(b and c), this highly local, and relatively small, perturbation induces nontrivial oscillations throughout the computational domain in a relatively short span of computational time. This strongly indicates transverse instability. We point out that nonlocality of (25) and the lack of localization in each direction of the solitons means an analytic study of stability is challenging. This is a subject of future interest, but is currently beyond the scope of the current paper.

The numerical simulations were done using a pseudospectral method in space and the ETDRK4 method [50, 51] in time. As (21) is nonlocal in η, and likewise the rescaled version (25) as well, we must determine how to numerically deal with the operator ∂_η^{-1}. To do this, in (21), we see for all time that

$$\left(-\frac{1}{2}\partial_Y^2 + \frac{1}{8}\partial_Y^4\right) \int_{\mathbb{R}} d\eta \bar{a}_0(\eta, Y, \bar{Z}) = 0,$$

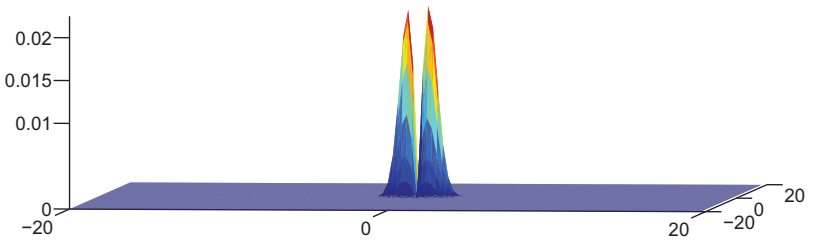

(a) Amplitude of a typical random perturbation used to introduce transverse components to the one-dimensional solution to (25).

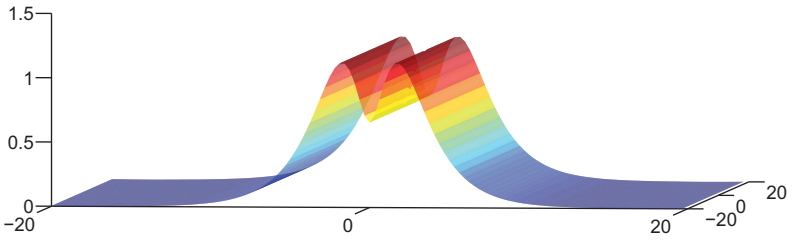

(b) Plot of perturbed solution to (25) at z = .26. z =

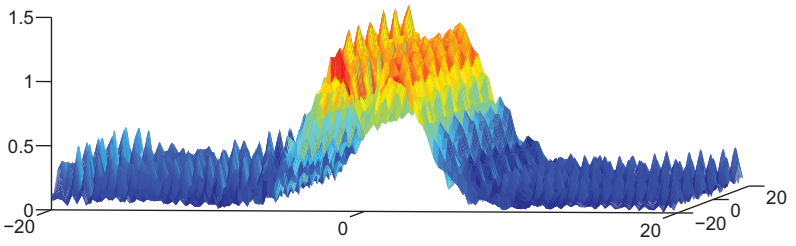

(c) Plot of perturbed solution to (25) at z = .5.

Figure 4. Perturbation and solution to (25) at $z = 0.26$ and $z = 0.5$, with $\nu = \sigma = 1$. The highly localized perturbation has induced oscillations throughout the entire domain on timescales much shorter than the reciprocal of the amplitude of the perturbation. (a) Amplitude of a typical random perturbation used to introduce transverse components to the one-dimensional solution to (25), (b) plot of perturbed solution to (25) at $z = 0.26$,Plot of perturbed solution to (25) at $z = 0.5$.

which immediately yields

$$\int_{\mathbb{R}} d\eta \bar{a}_0(\eta, Y, \tilde{Z}) = C_0(\bar{Z}) + C_1(\bar{Z})Y + C_2(\bar{Z})e^{2Y} + C_3(\bar{Z})e^{-2Y}. \qquad (26)$$

Requiring boundedness in Y shows $C_j(\bar{Z}) = 0$ in (26) for $j > 0$, and if we look at localized solutions in Y, then we must have $C_0(\bar{Z}) = 0$ as well. Thus, for two-dimensional localized profiles, we must have

$$\int_{\mathbb{R}} d\eta \bar{a}_0(\eta, Y, \bar{Z}) = 0.$$

However, if we do not have localization in both directions, then generally we see that the solution has nonzero average in η. As the initial conditions used throughout the semilocalized gap soliton simulations do not have zero η average, define ∂_η^{-1} via the formula

$$\partial_\eta^{-1} f = \frac{1}{2}\int_{-\infty}^{\eta} f(s)ds - \frac{1}{2}\int_{\eta}^{\infty} f(s)ds.$$

See Ref. [52], which outlines how to implement this operator in a pseudospectral way.

3. Dirac systems for real-mass potentials

As shown in Section 2, real-mass potentials at the order of the tight-binding limit do not introduce new terms in the dynamics. Therefore, a more careful approach is necessary to study this case. To do this, assuming no strain so that $\rho = 1$, for the NLS Equation (1), we use the approximation to the solution $u(x, y, z)$

$$u(x, y, z) = \vartheta\left(A(\mathbf{R}, Z)\bar{\varphi}_0(\mathbf{r}; \vartheta) + B(\mathbf{R}, Z)\bar{\varphi}_1(\mathbf{r}; \vartheta)\right) e^{i\mathbf{K}\cdot\mathbf{r} - i(\mu_0(\mathbf{K}) - \vartheta^2\alpha)z},$$

where $\mathbf{R} = \vartheta^{3/2}\mathbf{r}$, $Z = \vartheta^2 z$, α is given in (9), and the eigenvectors $\bar{\varphi}_j(\mathbf{r}; \vartheta)$ solve

$$H_\vartheta(\mathbf{K})\bar{\varphi}_j(\mathbf{r}; \vartheta) = \mu_j(\mathbf{K}, \vartheta)\bar{\varphi}_j(\mathbf{r}; \vartheta).$$

Again, we note the small amplitude and slow variation assumptions in the above ansatz. As we show, this allows us to maintain the localization in wave number around the Dirac point. Plugging this ansatz into the NLS equation, we then get, by using (7) and (8)

$$\begin{aligned} i\bar{\varphi}_0\partial_Z A + i\bar{\varphi}_1\partial_Z B = &-\tilde{\Delta}_T A\bar{\varphi}_0 + \tilde{\Delta}_T B\bar{\varphi}_1 \\ &-\frac{2}{\vartheta^{1/2}}e^{-i\mathbf{K}\cdot\mathbf{r}}\left(\nabla_{\mathbf{R}} A\cdot\nabla_{\mathbf{r}}(\bar{\varphi}_0 e^{i\mathbf{K}\cdot\mathbf{r}}) + \nabla_{\mathbf{R}} B\cdot\nabla_{\mathbf{r}}(\bar{\varphi}_1 e^{i\mathbf{K}\cdot\mathbf{r}})\right) \\ &+\sigma\left|A\bar{\varphi}_0 + B\bar{\varphi}_1\right|^2\left(A\bar{\varphi}_0 + B\bar{\varphi}_1\right) \\ &-\vartheta\bar{\varphi}_0\Delta_{\mathbf{R}} A - \vartheta\bar{\varphi}_1\Delta_{\mathbf{R}} B. \end{aligned}$$

Note, we have suppressed the explicit dependence on ϑ when writing $\bar{\varphi}_j(\mathbf{r};\vartheta)$ for readability.

Letting the unperturbed eigenvectors at $\mathbf{K}$ be denoted as $\bar{\varphi}_{0,0}(\mathbf{r})$ and $\bar{\varphi}_{1,0}(\mathbf{r})$, i.e.

$$H_0(\mathbf{K})\bar{\varphi}_{j,0} = \mu_0(\mathbf{K})\bar{\varphi}_{j,0},$$

we define P_0 to be the orthogonal projection onto the space spanned by $\bar{\varphi}_{j,0}$, and we define the operator

$$R_0 = (H_0(\mathbf{K}) - \mu_0(\mathbf{K}))^{-1}(1 - P_0).$$

As shown in Ref. [37], the perturbed eigenvectors, $\bar{\varphi}_0(\mathbf{r};\vartheta)$ and $\bar{\varphi}_1(\mathbf{r};\vartheta)$ become

$$\bar{\varphi}_j(\mathbf{r};\vartheta) \sim \tilde{c}_j(\vartheta)\left(e^{i\theta_j}\bar{\varphi}_{0,0} + \bar{\varphi}_{1,0} + \mathcal{H}(\vartheta)\left(e^{i\theta_j}\bar{\varphi}_{0,0} + \bar{\varphi}_{1,0}\right)\right). \tag{27}$$

where

$$\tilde{c}_j(\vartheta) \sim \left(2 + \left|\left|\mathcal{H}(\vartheta)(e^{i\theta_j}\bar{\varphi}_{0,0} + \bar{\varphi}_{1,0})\right|\right|_{2,p}^2\right)^{-1/2}, \tilde{\mathcal{H}}(\vartheta) = -i\vartheta R_0 W,$$

and

$$\theta_0 \sim \theta_1 + \pi, \tilde{\theta}_1 \sim \arg\left\{\left\langle R_0 W\bar{\varphi}_{1,0}, W\bar{\varphi}_{0,0}\right\rangle_p\right\}. \tag{28}$$

Again, the detuning parameter, $\tilde{\Delta}_T$, is found from

$$\tilde{\Delta}_T = \left|\left\langle R_0 W\bar{\varphi}_{1,0}, W\bar{\varphi}_{0,0}\right\rangle_p\right|. \tag{29}$$

From (27) and (28), we readily see that

$$\langle\bar{\varphi}_0(\cdot;\vartheta), \bar{\varphi}_1(\cdot,\vartheta)\rangle_p \sim i\vartheta^2 \mathrm{Im}\left\{e^{i\theta_0}\left\langle R_0 W\bar{\varphi}_{0,0}, R_0 W\bar{\varphi}_{1,0}\right\rangle_p\right\}.$$

Taking inner products with respect to $\bar{\varphi}_0(\mathbf{r};\vartheta)$ and $\bar{\varphi}_1(\mathbf{r};\vartheta)$, and using (27, 28), and the facts, shown in Ref. [15], that for an arbitrary vector $\mathbf{w} = (w_1, w_2)$,

$$\left\langle\bar{\varphi}_{j,0}e^{i\mathbf{K}\cdot\mathbf{r}}, \mathbf{w}\cdot\nabla_{\mathbf{r}}\left(\bar{\varphi}_{j,0}e^{i\mathbf{K}\cdot\mathbf{r}}\right)\right\rangle_p = 0,$$

and

$$\left\langle\bar{\varphi}_{0,0}e^{i\mathbf{K}\cdot\mathbf{r}}, \mathbf{w}\cdot\nabla_{\mathbf{r}}\left(\bar{\varphi}_{1,0}e^{i\mathbf{K}\cdot\mathbf{r}}\right)\right\rangle_p = \frac{i}{2}\bar{\lambda}^*(w_1 + iw_2)$$

and ignoring for the moment any nonlinearities gives

$$i\partial_Z\begin{pmatrix}A\\B\end{pmatrix} = \begin{pmatrix}-\tilde{\Delta}_T & 0\\ 0 & \tilde{\Delta}_T\end{pmatrix}\begin{pmatrix}A\\B\end{pmatrix} + \begin{pmatrix}i\mathrm{Re}\{\bar{c}L\} & -\mathrm{Im}\{\bar{c}L\}\\ \mathrm{Im}\{\bar{c}L\} & -i\mathrm{Re}\{\bar{c}L\}\end{pmatrix}\begin{pmatrix}A\\B\end{pmatrix},$$

where

$$\bar{c} = \frac{\bar{\lambda}}{\vartheta^{1/2}}e^{-i\theta_0}, \tilde{L} = \partial_X - i\partial_Y.$$

Again, $\bar{\lambda}$ is the same as $\lambda_\sharp$ in Ref. [15]. Using (A.6) in the Appendix, we see that $\bar{\lambda} \sim i\sqrt{3}\ell a^{(tb)}/\rho = \mathcal{O}(\epsilon)$, where $a^{(tb)}$ is given by (A.7), and ϵ is the scale introduced by the tight-binding limit. We then, by choosing the well depth $1/h^2$ to be sufficiently large, take the balance

$$\frac{\bar{\lambda}}{\vartheta^{1/2}} \sim i\frac{\sqrt{3}\ell}{\rho}\frac{a^{(tb)}}{\vartheta^{1/2}} \equiv i\tilde{\lambda} = \mathcal{O}(1). \tag{30}$$

By introducing the transformation

$$\begin{pmatrix} \tilde{A} \\ \tilde{B} \end{pmatrix} = \frac{1}{\sqrt{2}}\begin{pmatrix} e^{-i\theta_0} & -e^{-i\theta_0} \\ 1 & 1 \end{pmatrix}\begin{pmatrix} A \\ B \end{pmatrix},$$

we take the linear problem to

$$i\partial_Z\begin{pmatrix} \tilde{A} \\ \tilde{B} \end{pmatrix} = \begin{pmatrix} 0 & \bar{c}_1(\partial_X - i\partial_Y) + \bar{c}_2 \\ -\bar{c}_1^*(\partial_X + i\partial_Y) + \bar{c}_2^* & 0 \end{pmatrix}\begin{pmatrix} \tilde{A} \\ \tilde{B} \end{pmatrix},$$

where

$$\bar{c}_1 = i\frac{\bar{\lambda}}{\vartheta^{1/2}}e^{-2i\theta_0} \sim -\tilde{\lambda}e^{-2i\theta_0}, \bar{c}_2 = \tilde{\Delta}_T e^{-i\theta_0}.$$

The dispersion relationship of this linear operator is given by

$$\omega(\tilde{\mathbf{k}}) = \pm\left|\bar{c}_1(i\tilde{k}_x + \tilde{k}_y) + \bar{c}_2\right|.$$

Therefore, we see the effect of the $\mathcal{PT}$ perturbation is to shift the position of the conical intersection in the slow modulation limit.

Introducing the transformation

$$\tilde{A} = \bar{A}e^{i\theta_\vartheta(X,Y)}, \tilde{B} = \bar{B}e^{i\theta_\vartheta(X,Y)},$$

where we choose the real-valued function θ_ϑ to satisfy

$$i\bar{c}_1(\partial_X - i\partial_Y)\theta_\vartheta + \bar{c}_2 = 0,$$

then gives us the linear system

$$i\partial_Z\begin{pmatrix} \bar{A} \\ \bar{B} \end{pmatrix} = \begin{pmatrix} 0 & \bar{c}_1(\partial_X - i\partial_Y) \\ -\bar{c}_1^*(\partial_X + i\partial_Y) & 0 \end{pmatrix}\begin{pmatrix} \bar{A} \\ \bar{B} \end{pmatrix}.$$

We thus get the dispersion relationship

$$\omega(\tilde{\mathbf{k}}) = \pm\left|\tilde{\lambda}\right|\left|\tilde{\mathbf{k}}\right|,$$

and so we have re-centered the dispersion relationship by taking out the shift introduced by the complex numbers $\bar{c}_1$ and $\bar{c}_2$.

In the tight-binding limit, see Refs. [11] and [12] for more details, the nonlinearities, after transformation are approximated by

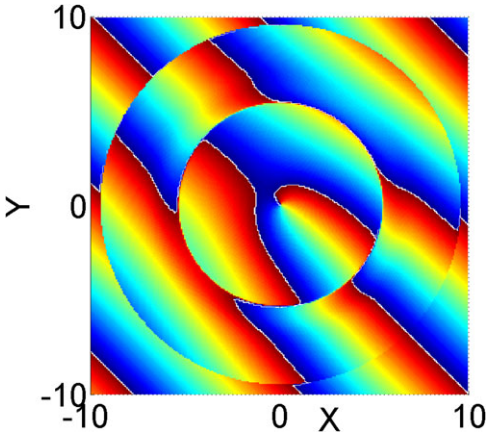

Figure 5. Plot of the phase of $\bar{B}(X, Y, 10)e^{i\theta_\vartheta(X,Y)}$ from (31) for $Z = 10$, $\theta_0 = \pi/4$, $\tilde{\lambda} = 1$, and $\sigma = 1$. The strong spatial variation and alignment with the angle θ_0 in the phase is due to the $\mathcal{PT}$ perturbation while the "pitchfork" at the center represents the impact of pseudospin [42].

$$\left\langle \left| \bar{A}\bar{\varphi}_{0,0} + \bar{B}e^{-2i\theta_0}\bar{\varphi}_{1,0} \right|^2 (\bar{A}\bar{\varphi}_{0,0} + \bar{B}e^{-2i\theta_0}\bar{\varphi}_{1,0}), \bar{\varphi}_{0,0} \right\rangle \sim g \left|\bar{A}\right|^2 \bar{A}$$

$$\left\langle \left| \bar{A}\bar{\varphi}_{0,0} + \bar{B}e^{-2i\theta_0}\bar{\varphi}_{1,0} \right|^2 (\bar{A}\bar{\varphi}_{0,0} + \bar{B}e^{-2i\theta_0}\bar{\varphi}_{1,0}), \bar{\varphi}_{1,0} \right\rangle \sim g \left|\bar{B}\right|^2 \bar{B},$$

where

$$g = \int_\Omega \left|\bar{\varphi}_{1,0}(\mathbf{r})\right|^4 d\mathbf{r}.$$

To leading order then, we have the nonlinear equation for the slowly evolving envelopes

$$i\partial_Z \begin{pmatrix} \bar{A} \\ \bar{B} \end{pmatrix} - \begin{pmatrix} 0 & \bar{c}_1(\partial_X - i\partial_Y) \\ -\bar{c}_1^*(\partial_X + i\partial_Y) & 0 \end{pmatrix} \begin{pmatrix} \bar{A} \\ \bar{B} \end{pmatrix} + \tilde{\sigma} \begin{pmatrix} \left|\bar{A}\right|^2 \bar{A} \\ \left|\bar{B}\right|^2 \bar{B} \end{pmatrix} = 0, \quad (31)$$

where $\tilde{\sigma} = g\sigma$. This is a nonlinear Dirac equation similar to that found in [11].

Therefore, the most striking effect of a $\mathcal{PT}$ perturbation on the long time dynamics of envelopes is the phase $\theta_\vartheta(X, Y)$. Using characteristic coordinates, we find that

$$\theta_\vartheta(X, Y) = \frac{1}{|\bar{c}_1|^2}\left(-\mathrm{Re}(\bar{c}_1\bar{c}_2^*)Y + \mathrm{Im}(\bar{c}_1\bar{c}_2^*)X\right)$$

$$\sim \frac{\tilde{\Delta}_T}{\tilde{\lambda}}\left(\cos(\theta_0)Y + \sin(\theta_0)X\right)$$

The effect of this phase can be seen in Figure 5. To generate this figure, we numerically solve (31) using a pseudo-spectral method in space and the ETDRK4 method in time. We take $\bar{A}(X, Y, 0) = e^{-(X^2+Y^2)}$ and $\bar{B}(X, Y, 0) = 0$,

we set $\theta_0 = \pi/4$, $\tilde{\lambda} = 1$, $\sigma = 1$, and we run our simulations out to $Z = 10$. As can be seen in Figure 5, the added phase introduced by a real-mass potential induces a rotation, given by θ_0, in the phase, and it also introduces a nontrivial spatial structure.

In physical terms, the impact of the additional phase is to impart momentum on the propagating beam. One can see this by looking at the average value of the momentum operator [53] $\hat{p} = -i\nabla$ (note, we have taken Planck's constant to be unity). For a solution u to the NLS equation, we can write

$$u = \sqrt{\tilde{\rho}} e^{i\theta},$$

which is the Madelung transformation [53] where we treat $\tilde{\rho}$ as the "density" and $\mathbf{V} = \nabla\theta$ as the "velocity" of the solution u. We readily see that the average value of the momentum operator is then given by

$$\langle u \,|\hat{p}|\, u \rangle = \int_{\mathbb{R}^2} \tilde{\rho} \nabla\theta \, d\mathbf{r},$$

where we have used Dirac's "bra" and "ket" notation to conform to standard presentations of quantum mechanics. Therefore, the phase introduced by a real-mass $\mathcal{PT}$ perturbation imparts an average momentum term, say $\mathbf{p}_{PT}$, equal to

$$\mathbf{p}_{PT} \sim \frac{\tilde{\Delta}_T}{\tilde{\lambda}} \vartheta^{3/2} \left(\int_{\mathbb{R}^2} |u|^2 d\mathbf{r} \right) (\sin(\theta_0), \cos(\theta_0)),$$

where θ_0, $\tilde{\Delta}_T$, and $\tilde{\lambda}$ are given by (28, 29), and (30), respectively. Thus, by engineering the $\mathcal{PT}$ perturbation, both the magnitude and direction of this momentum contribution can be controlled. This added momentum would complement the angular momentum introduced by the, now experimentally verified [42], pseudo-spin imparted by the honeycomb lattice. The impact of pseudospin can be seen in the "pitchfork" at the center of Figure 5; we refer to Ref. [42] for more details. Both of these sources of momentum could potentially be used in controlling the flow of light novel ways.

4. Conclusions

In this paper, we have shown how to derive nonlinear wave equations describing the effective dynamics in $\mathcal{PT}$-symmetric honeycomb lattices with nonlinearity. For the two classes of $\mathcal{PT}$-perturbations studied, in the imaginary-mass case we find via a tight-binding approximation the necessary conditions to avoid phase transitions by introducing strain into the lattice. We then, by taking a continuum limit, find nonlinear dispersive wave equations which describe the dynamics of waves propagating in a system where strain and the imaginary mass potential are

in asymptotic balance. We show that $\mathcal{PT}$-perturbations have a localizing effect. Semilocalized gap solitons are found in this system, representing a nontrivial impact of nonlinearity. In the case of real-mass potentials, we find a nonlinear Dirac equation describes dynamics to leading order. We show that real-mass potentials introduce nontrivial spatially varying phase effects, which implies real-mass potentials could have impacts in emerging areas of modern physics.

5. Acknowledgments

The authors would like to thank Mark Ablowitz, Jianke Yang, and Zhigang Chen for many illuminating discussions. We would also like to thank the reviewers for their very useful comments and suggestions. Yi Zhu was partially supported by NSFC under grant no. 11204155, Tsinghua University Initiative Scientific Research Program under grant nos. 20121087902, 20131089184.

Appendix A: Background on tight-binding approximations

Here, we collect the facts that are necessary to understand the tight-binding approximations used throughout the text. As each well $\mathbf{r}_j$ of $V(\mathbf{r})$ is by construction a local minima, we further suppose they are nondegenerate so that $V''(\mathbf{r}_j) > 0$. We let $V''(\mathbf{r}_1) = \tilde{U}^{-1}\Lambda\tilde{U}$, and let $\mathbf{y} = \tilde{U}\mathbf{r}$ where $\tilde{U}$ is unitary and Λ is diagonal since $V''(\mathbf{r}_1)$ is self-adjoint. We define the harmonic oscillator problem

$$-\Delta_{\mathbf{y}}\phi^{(osc)} + \mathbf{y}^T\Lambda\mathbf{y}\phi^{(osc)} = E_n\phi^{(osc)}, \tag{A.1}$$

where E_n are the ordered values ($E_n < E_{n+1}$) of the set

$$\left\{\sqrt{\Lambda_1}(2j+1) + \sqrt{\Lambda_2}(2k+1),\, j \geq 0, k \geq 0\right\}.$$

with Λ_j being the nonzero entries in the diagonal matrix Λ. For example, $E_0 = \sqrt{\Lambda_1} + \sqrt{\Lambda_2}$. We then have the following theorem:

THEOREM 2. *[47, 54] Choosing some integer n, for sufficiently small h, there are n eigenvalues of L_{or} below its continuous spectra such that $\tilde{E}_n$ has the expansion*

$$\tilde{E}_n = \frac{E_n}{h} + \mathcal{O}(h^{-1/2}),$$

where E_n is defined in (A.1).

Likewise, in [55], one has on a neighborhood around $\mathbf{r}_1$ that $\phi^{(osc)}$ is a leading order approximation to $\phi_1^{(or)}$ as $h \to 0$. Further, as shown in [55], $\phi_1^{(or)}$ is exponentially localized, and thus to leading order, in a neighborhood around

$\mathbf{r}_1$, we may take $\phi^{(or)}$ to be real and even. See also Ref. [11] where these approximations are written in explicit and detailed form.

Computations for the real-mass potential

In order to show the results in Section 3, we wish to show how to approximate the following terms,

$$\left\langle \nabla(e^{i\mathbf{K}\cdot\mathbf{r}}\bar{\varphi}_{j,0}(\cdot,\mathbf{K})), e^{i\mathbf{K}\cdot\mathbf{r}}\bar{\varphi}_{j,0}(\cdot,\mathbf{K})\right\rangle_p, \tag{A.2}$$

for $j = 0, 1$ and

$$\left\langle \mathbf{w}\cdot\nabla(e^{i\mathbf{K}\cdot\mathbf{r}}\bar{\varphi}_{0,0}(\cdot,\mathbf{K})), e^{i\mathbf{K}\cdot\mathbf{r}}\bar{\varphi}_{1,0}(\cdot,\mathbf{K})\right\rangle_p, \tag{A.3}$$

using tight-binding arguments. To deal with (A.2), we note that for $j = 0$, using (A.4) at $\mathbf{k} = \mathbf{K}$ to approximate $\bar{\varphi}_{0,0}$, that

$$\begin{aligned}\left\langle \nabla(e^{i\mathbf{K}\cdot\mathbf{r}}\bar{\varphi}_{0,0}), e^{i\mathbf{K}\cdot\mathbf{r}}\bar{\varphi}_{0,0}\right\rangle_p &= \sum_{\mathbf{v}}\sum_{\mathbf{p}} e^{i\mathbf{K}\cdot(\mathbf{v}-\mathbf{p})}\int_\Omega \nabla\phi_1^{(or)}(\mathbf{r}-\mathbf{v})\phi_1^{(or)}(\mathbf{r}-\mathbf{p})d\mathbf{r}\\ &\sim \sum_{\mathbf{v}}\int_\Omega \nabla\phi_1^{(or)}(\mathbf{r}-\mathbf{v})\phi_1^{(or)}(\mathbf{r}-\mathbf{v})d\mathbf{r}\\ &\sim \int_{\mathbb{R}^2}\nabla\phi_1^{(or)}(\mathbf{r})\phi_1^{or}(\mathbf{r})d\mathbf{r}\\ &\sim 0.\end{aligned}$$

An identical argument takes care of the $j = 1$ case. Note, we have suppressed the explicit dependence of $\mathbf{K}$ in $\bar{\varphi}_{j,0}(\mathbf{r},\mathbf{K})$ for readability.

The first two Bloch functions are well-approximated by the expansions

$$\tilde{\varphi}_0(\mathbf{r};\mathbf{k}) = \frac{1}{\sqrt{2}}\sum_{\mathbf{v}}\left(-t_{00}(\mathbf{k})\phi_{1,\mathbf{v}}^{(or)}(\mathbf{r}) + t_{01}(\mathbf{k})\phi_{2,\mathbf{v}}^{(or)}(\mathbf{r})\right)e^{i\mathbf{k}\cdot\mathbf{v}}, \tag{A.4}$$

$$\tilde{\varphi}_1(\mathbf{r};\mathbf{k}) = \frac{1}{\sqrt{2}}\sum_{\mathbf{v}}\left(t_{10}(\mathbf{k})\phi_{1,\mathbf{v}}^{(or)}(\mathbf{r}) + \phi_{2,\mathbf{v}}^{(or)}(\mathbf{r})\right)e^{i\mathbf{k}\cdot\mathbf{v}}, \tag{A.5}$$

where, if $\rho > 1/2$,

$$t_{00}(\mathbf{k}) = \begin{cases}\dfrac{\gamma(\mathbf{k})}{|\gamma(\mathbf{k})|} & \mathbf{k}\neq\mathbf{K}_\rho,\mathbf{K}_\rho',\\[2ex] 1 & \mathbf{k}=\mathbf{K}_\rho,\mathbf{K}_\rho',\end{cases}$$

$$t_{01}(\mathbf{k}) = \begin{cases}1 & \mathbf{k}\neq\mathbf{K}_\rho,\mathbf{K}_\rho',\\[2ex] 0 & \mathbf{k}=\mathbf{K}_\rho,\mathbf{K}_\rho',\end{cases}\qquad \tilde{t}_{10}(\mathbf{k}) = \begin{cases}\dfrac{\gamma(\mathbf{k})}{|\gamma(\mathbf{k})|} & \mathbf{k}\neq\mathbf{K}_\rho,\mathbf{K}_\rho',\\[2ex] 0 & \mathbf{k}=\mathbf{K}_\rho,\mathbf{K}_\rho',\end{cases}$$

where $\mathbf{K}_\rho$ is given by (17). If $\rho < 1/2$, or under significant strain, the bands separate and $t_{00}(\mathbf{k}) = \gamma(\mathbf{k})/|\gamma(\mathbf{k})|$, $t_{01}(\mathbf{k}) = 1$, and $t_{10}(\mathbf{k}) = \gamma(\mathbf{k})/|\gamma(\mathbf{k})|$ for all $\mathbf{k}$. So for (A.3), taking $\rho = 1$, we see that, taking into account the relative proximity of nearest neighbors at $\mathbf{p} = \mathbf{v}$, $\mathbf{p} = \mathbf{v} - \mathbf{v}_1$, and $\mathbf{p} = \mathbf{v} - \mathbf{v}_2$, and using (A.4) and (A.5) to approximate $\phi_{j,0}$,

$$\begin{aligned}\left\langle \nabla(e^{i\mathbf{K}\cdot\mathbf{r}}\bar{\varphi}_{0,0}), e^{i\mathbf{K}\cdot\mathbf{r}}\bar{\varphi}_{1,0}\right\rangle_p &= \sum_{\mathbf{v}}\sum_{\mathbf{p}} e^{i\mathbf{K}\cdot(\mathbf{v}-\mathbf{p})}\int_\Omega \nabla\phi_1^{(or)}(\mathbf{r}-\mathbf{v})\phi_2^{(or)}(\mathbf{r}-\mathbf{p})d\mathbf{r}\\ &\sim \int_{\mathbb{R}^2}\nabla\phi_1^{(or)}(\mathbf{r})\phi_2^{(or)}(\mathbf{r})d\mathbf{r}\\ &\quad + {}^{i\mathbf{K}\cdot\mathbf{v}_1}\int_{\mathbb{R}^2}\nabla\phi_1^{(or)}(\mathbf{r})\phi_2^{(or)}(\mathbf{r}+\mathbf{v}_1)d\mathbf{r}\\ &\quad + e^{i\mathbf{K}\cdot\mathbf{v}_2}\int_{\mathbb{R}^2}\nabla\phi_1^{(or)}(\mathbf{r})\phi_2^{(or)}(\mathbf{r}+\mathbf{v}_2)d\mathbf{r}\end{aligned}$$

We note that

$$\begin{aligned}\int_{\mathbb{R}^2}\nabla\phi_1^{(or)}(\mathbf{r})\phi_1^{(or)}(\mathbf{r}+\mathbf{v}_j-\mathbf{d})d\mathbf{r} &= \int_{\mathbb{R}^2}\nabla\phi_1^{(or)}(\mathbf{r}-\mathbf{v}_j)\phi_2^{(or)}(\mathbf{r})d\mathbf{r}\\ &= \int_{\mathbb{R}^2}\nabla\phi_1^{(or)}(\mathbf{r})\phi_2^{(or)}(\mathbf{r})d\mathbf{r}\\ &\quad - \int_{\mathbb{R}^2} D_2\phi_1^{(or)}\mathbf{v}_j\phi_2^{(or)}(\mathbf{r})d\mathbf{r}+\cdots\end{aligned}$$

where for the Hessian $D_2\phi_1^{(or)}$, we take

$$D_2\phi_1^{(or)}(\mathbf{r}) \sim \partial_x^2\phi_1^{(or)}(\mathbf{r})I,$$

with I being the 2×2 identity. This then shows that

$$\left\langle \mathbf{w}\cdot\nabla(e^{i\mathbf{K}\cdot\mathbf{r}}\bar{\varphi}_{0,0}), e^{i\mathbf{K}\cdot\mathbf{r}}\bar{\varphi}_{1,0}\right\rangle_p \sim \frac{\sqrt{3}\ell a^{(tb)}}{2\rho}(w_1 - iw_2), \tag{A.6}$$

where we have used $\mathbf{w} = (w_1, w_2)$ and

$$a^{(tb)} = \int_{\mathbb{R}^2}\partial_x^2\phi_1^{(or)}(\mathbf{r})\phi_2^{(or)}(\mathbf{r})d\mathbf{r}. \tag{A.7}$$

This result is consistent with the results found in Refs. [11] and [15]. We also note in the tight-binding limit ($h \to 0$) that $a^{(tb)} \to 0$.

References

1. O. Peleg, G. Bartal, B. Freedman, O. Menla, M. Segev, and D. N. Christodoulides, Conical diffraction and gap solitons in honeycomb photonic lattices, *Phys. Rev. Lett.* 98: 103901 (2007).
2. M. C. Rechtsman, J. M. Zeuner, M. Heinrich, A. Tünnermann, M. Segev, and A. Szameit, Strain-induced pseudomagnetic field and Landau levels in photonic structures, *Nat. Photon*. 7:153–158(2013).
3. M. C. Rechtsman, Y. Plotnik, J. M. Zeuner, A. Szameit, and M. Segev, Topological creation and destruction of edge states in photonic graphene, *Phys. Rev. Lett.* 111: 103901, 2013.
4. M. C. Rechtsman, J. M. Zeuner, Y. Plotnik, Y. Lumer, S. Nolte, F. Dreisow, M. Segev, and A. Szameit, Photonic Floquet topological insulators, *Nature* 496: 196–200, 2013.
5. Y. Plotnik, M. C. Rechtsman, D. Song, M. Heinrich, J. M. Zeuner, S. Nolte, Y. Lumer, N. Malkova, J. Xu, A. Szameit, Z. Chen, and M. Segev. Observation of unconventional edge states in 'photonic graphene'. *Nat. Mat.* 13: 57–62, 2013.
6. S. R. Zanderbergen and M. J. A. deDood. Experimental observation of strong edge effects on the pseudodiffusive transport of light in photonic graphene. *Phys. Rev. Lett.* 104: 043903, 2010.
7. S. Bittner, B. Dietz, M. Miski-Oglu, P. Oria Iriarte, A. Richter, and F. Schäfer. Observation of a dirac point in microwave experiments with a photonic cyrstal modeling graphene. *Phys. Rev. B* 82: 014301, 2010.
8. U. Kuhl, S. Barkhofen, T. Tudorovskiy, H. J. Stöckman, and T. Hossain. Dirac point and edge states in a microwave realization of tight-binding graphene-like structures. *Phys. Rev. B* 82: 094308, 2010.
9. M. Bellec, U. Kuhl, G. Montambaux, and F. Mortessagne. Tight-binding couplings in microwave artificial graphene. *Phys. Rev. B* 88: 115437, 2013.
10. M. Bellec, U. Kuhl, G. Montambaux, and F. Mortessagne. Topological transition of Dirac points in a microwave experiment. *Phys. Rev. Lett.* 110: 033902, 2013.
11. M. J. Ablowitz and Y. Zhu. Evolution of Bloch-mode envelopes in two-dimensional generalized honeycomb lattices. *Phys. Rev. A* 82: 013840, 2010.
12. M. J. Ablowitz, C. W. Curtis, and Y. Zhu. On tight-binding approximations in optical lattices. *Stud. Appl. Math.* 129: 362–388, 2012.
13. M. J. Ablowitz, S. Nixon, and Y. Zhu. Conical diffraction in honeycomb lattices. *Phys. Rev. A* 79: 053830, 2009.
14. L. H. Haddad and L. C. Carr. The nonlinear Dirac equation in Bose–Einstein condensates: Foundation and symmetries. *Physica D* 238: 1413–1421, 2009.
15. C. L. Fefferman and M. I. Weinstein. Honeycomb lattice potentials and Dirac points. *J. Am. Math. Soc.* 25: 1169–1220, 2012.
16. C. L. Fefferman and M. I. Weinstein. Wave packets in honeycomb structures and two-dimensional Dirac equations. *Comm. Math. Phys.* 326: 251–286, 2014.
17. C. L. Fefferman, J. P. Lee-Thorp, and M. I. Weinstein. Topologically protected states in one-dimensional continuous systems and Dirac points. *PNAS* 111: 8759–8763, 2014.
18. F. D. M Haldane and S. Raghu. Possible realization of directional optical wavesguides in photonic crystals with broken time-reversal symmetry. *Phys. Rev. Lett.* 100: 013904, 2008.
19. S. Raghu and F. D. M Haldane. Analogs of quantum-Hall-effect edges states in photonic crystals. *Phys. Rev. A* 78: 033834, 2008.
20. C. M. Bender and S. Boettcher. Real spectra in non-Hermitian Hamiltonians having PT symmetry. *Phys. Rev. Lett.* 80: 5243–5246, 1998.

21. I. V. Barashenkov, L. Baker, and N. V. Alexeeva. PT-symmetry breaking in a necklace of coupled optical waveguides. *Phys. Rev. A* 87: 033819, 2013.
22. A. Ruschhaupt, F. Delgado, and J. G. Muga. Physical realization of PT-symmetric potential scattering in a planar slab waveguide. *J. Phys. A* 38: L171–L176, 2005.
23. R. El Ganainy, K. G. Makris, D. N. Christodoulides, and Z. H. Musslimani. Theory of coupled optical PT symmetric structures. *Opt. Lett.* 32: 3185, 2007.
24. K. G. Makris, R. El Ganainy, D. N. Christodoulides, and Z. H. Musslimani. Beam dynamics in PT symmetric optical lattices. *Phys. Rev. Lett*. 100: 103904, 2008.
25. C. E. Rüter, K. G. Makris, R. El-Ganainy, D. N. Christodoulides, M. Segev, and D. Kip. Observation of parity-time symmetry in optics. *Nat. Phys*. 6: 192–195, 2010.
26. A. Guo, G. J. Salamo, D. Duchesne, R. Morandotti, M. Volatier-Ravat, V. Aimez, G. A. Siviloglou, and D. N. Christodoulides. Observation of PT-symmetry breaking in complex optical potentials. *Phys. Rev. Lett*. 103: 093902, 2009.
27. Z. Lin, H. Ramezani, T. Eichelkraut, T. Kottos, H. Cao, and D. N. Christodoulides. Unidirectional invisibility induced by PT-symmetric periodic structures. *Phys. Rev. Lett*. 106: 213901, 2011.
28. K. G. Makris, R. El-Ganainy, D. N. Christodoulides, and Z. H. Musslimani. PT-symmetric periodic optical potentials. *Int. J. Theor. Phys*. 50: 1019–1041, 2011.
29. S. Nixon, L. Ge, and Y. Yang. Stability analysis for solitons in PT-symmetric optical lattices. *Phys. Rev. A* 85: 023822, 2012.
30. D. E. Pelinovsky, P. G. Kevrekidis, and D. J. Frantzeskakis. PT-symmetric lattices with spatially extended gain/loss are generically unstable. *Europhys. Lett*. 101: 11002, 2013.
31. E. Caliceti and S. Graffi. Reality and non-reality of the spectrum of PT-symmetric operators: Operator-theoretic criteria. *Pramana* 73: 241–249, 2009.
32. E. Caliceti, S. Graffi, and J. Sjöstrand. Spectra of PT-symmetric operators and perturbation theory. *J. Phys. A* 38: 185–193, 2005.
33. E. Caliceti, S. Graffi, and J. Sjöstrand. PT-symmetric non-self adjoint operators, diagonalizable and non-diagonalizable, with a real discrete spectrum. *J. Phys. A* 40: 10155–10170, 2007.
34. H. Ramezani, T. Kottos, V. Kovanis, and D. N. Christodoulides. Exceptional-point dynamics in photonic honeycomb lattices with PT symmetry. *Phys. Rev. A* 85: 013818, 2012.
35. A. Szameit, M. C. Rechtsman, O. Bahat-Treidel, and M. Segev. PT-symmetry in honeycomb photonic lattices. *Phys. Rev. A* 84: 021806, 2011.
36. H. Schomerus and N. Y. Halpern. Parity anomaly and Landau-level laising in strained photonic honeycomb lattices. *Phys. Rev. Lett*. 110: 013903, 2013.
37. C. W. Curtis and M. J. Ablowitz. On the existence of real spectra in PT-symmetric honeycomb optical lattices. *J. Phys. A* 47: 225205, 2014.
38. M. J. Ablowitz and Y. Zhu. Nonlinear wave packets in deformed honeycomb lattices. *SIAM J. Appl. Math*. 73: 1959–1979, 2013.
39. G. Agrawal and Y. S. Kivshar. *Optical Solitons: From Fibers to Photonic Crystals*. Academic Press, London, 2003.
40. M. Creutz. Emergent spin. *Ann. Phys*. 342: 21–30, 2014.
41. M. Mecklenburg and B. C. Regan. Spin and the honeycomb lattice: Lessons from graphene. *Phys. Rev. Lett*. 106: 116803, 2011.
42. D. Song, L. Tang, Y. Zhu, M. Ablowitz, V. Paltoglou, N. K. Efremidis, J. Xu, and Z. Chen. Direct observation of pseudospin-mediated vortex generation in photonic graphene. In *CLEO:QELS Fundamental Science*, 2014.
43. O. Bahat-Treidel, O. Peleg, M. Segev, and H. Buljan. Breakdown of Dirac dynamics in honeycomb lattices due to nonlinear interactions. *Phys. Rev. A* 82: 013830, 2010.

44. M. J. Ablowitz and Y. Zhu. Nonlinear diffraction in photonic graphene. *Opt. Lett*. 36: 762–764, 2011.
45. M. Reed and B. Simon. *Methods of Mathematical Physics IV: Analysis of Operators*. Academic Press, New York, NY, 1978.
46. P. D. Hislop and I. M. Sigal. *Introduction to Spectral Theory with Applications to Schrödinger Operators*. Springer, New York, NY, 1996.
47. M. Dimassi and J. Sjöstrand. *Spectral Asymptotics in the Semi-Classical Limit*. Cambridge University Press, Cambridge, 1999.
48. D. C. Calvo and T. R. Akylas. On the formation of bound states by interacting solitary waves. *Physica D* 101: 270–288, 1997.
49. J. Yang and T. R. Akylas. Continuous families of embedded solitons in the third-order nonlinear Schrödinger equation. *Stud. Appl. Math*. 111: 359–375, 2003.
50. S. M. Cox and P. C. Matthews. Exponential time differencing for stiff systems. *J. Comput. Phys*. 176: 430–455, 2002.
51. A. K. Kassam and L. N. Treffethen. Fourth-order time-stepping for stiff pdes. *SIAM J. Sci. Comput*. 26: 1214–1233, 2006.
52. M. J. Ablowitz and C. W. Curtis. Conservation laws and web-solutions for the Benney–Luke equation. *Proc. Roy. Soc. A* 2151: 20120690, 2013.
53. J. J. Sakurai. *Modern Quantum Mechanics*, revised ed. Addison-Wesley, Boston, MA, 1994.
54. B. Simon. Semiclassical analysis of low lying eigenvalues I: Non-degenerate minima: Asymptotic expansions. *Ann. Inst. Henri Poincaré* 38: 295–308, 1983.
55. B. Helffer. *Introduction to the Semi-classical Analysis for the Schrödinger Operator and Applications*. Springer, Berlin, 1986. San Diego State University Tsinghua University

San Diego State University
Zhou Pei-Yuan Center for Applied Mathematics, Tsinghua University

(Received August 22, 2014)